

# DIFFUSION-BASED NEURAL NETWORK WEIGHTS GENERATION

**Anonymous authors**

Paper under double-blind review

## ABSTRACT

Transfer learning, while fundamental to modern deep learning, faces critical limitations in model selection and storage requirements. To address these challenges, we introduce D2NWG: Diffusion-based Neural Network Weights Generation, a diffusion framework that learns to generate task-specific neural network weights by modeling the distribution of weights from diverse pretrained models. Our approach conditions the diffusion process on dataset features, task descriptions, and architectural specifications, enabling direct generation of task-specific weights without the need to store and search through extensive model collections. Comprehensive experiments validate D2NWG’s effectiveness across multiple scenarios: it matches or exceeds traditional pretrained models on in-distribution tasks, provides superior initialization for novel domains with faster convergence, and achieves a 6% improvement in few-shot learning scenarios. Through extensive ablation studies, we demonstrate that D2NWG’s performance scales with the diversity and size of its training set. D2NWG shows particular promise in large language model applications, enabling efficient exploration of pretrained parameter spaces without the computational burden of traditional fine-tuning. In rigorous evaluations on the OpenLM leaderboard, our approach improved LLaMA-3-2-1B-instruct performance by 3% on challenging mathematical reasoning tasks, with a consistent 0.36% gain across all benchmarks. These results establish D2NWG as a versatile and powerful framework for neural network weight generation, offering a practical solution to the challenges of traditional transfer learning.

## 1 INTRODUCTION

Diffusion-based generative models have emerged as a breakthrough technology in artificial intelligence, achieving state-of-the-art performance in generating complex, high-dimensional data across domains including natural language, audio, images, and video (Gozalo-Brizuela & Garrido-Merchán, 2023). The success of these models stems from their principled approach to data generation through iterative denoising (Ho et al., 2020b; Rombach et al., 2022; Peebles & Xie, 2023; Gao et al., 2023), which has proven remarkably effective for modeling complex probability distributions and generating high-quality samples (Yang et al., 2024).

Despite these advances in data generation, a fundamental challenge remains under-explored: can we leverage the powerful framework of diffusion models to generate neural network weights themselves from pretrained models? This capability would transform key machine learning paradigms, particularly in transfer learning and AutoML (Hutter et al., 2019; Doke & Gaikwad, 2021). By directly generating task-tailored network parameters, we could potentially bypass the computational overhead of traditional fine-tuning while achieving superior adaptation to novel tasks.

Recent attempts at weight generation through generative hyper-representation learning (Schürholt et al., 2022a) have only scratched the surface of this challenge. Current approaches, including latent diffusion (Wang et al., 2024) and kernel density estimation methods Schürholt et al. (2024), are severely constrained in both scope and capability - limited to small architectures and lacking cross-dataset knowledge transfer. Most critically, these methods focus exclusively on unconditional generation within known distributions, failing to address the core challenge of generating task-specific weights for novel problems from diverse pretrained models’ weights distribution. Although proven to improve the performance on seen tasks, this limitation fundamentally restricts their utility for

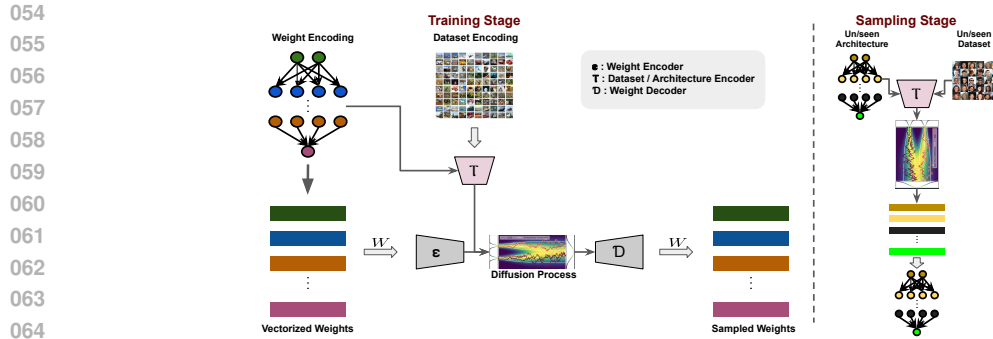


Figure 1: **Stage 1:** VAE Encoder and Decoder training process. **Stage 2:** dataset encoder training stage. **Stage 3:** Dataset conditioned diffusion process.

practical applications in model selection and transfer learning, where weights task-tailored weights generation and adaptation to unseen tasks are essential. Although recent meta-learning approaches by Nava et al. (2023) and Zhang et al. (2024) have advanced weight generation for visual and few-shot tasks, they fall short of providing truly dataset-specific solutions.

To address these challenges, we introduce Diffusion-based Neural Network Weight Generation (D2NNG), a novel approach that leverages latent diffusion to generate neural network parameters by learning from diverse pretrained model weights. Our method reimagines the latent diffusion paradigm for weight generation by incorporating robust dataset and task conditioning capabilities. D2NNG learns weight distributions from a collection of models pretrained across varied datasets, conditioned on dataset or task description enabling task-specific weights generation. The scalability and versatility of D2NNG represent a significant advancement in neural network weight generation. Our analysis reveals that the diversity and size of the pretrained model training set strongly correlates with improved generalization to unseen datasets and tasks. A key strength of D2NNG is its ability to learn the distribution of weights from diverse model architectures and pretraining datasets, and then generate new weights that maintain performance comparable to individual pretrained models on in-distribution tasks.

Our empirical evaluation validates the contribution of D2NNG as follows:

- The generated weights match or outperform traditional pretrained models on seen tasks while enabling faster, better learning on new tasks through superior weight initialization.
- D2NNG outperforms recent meta-learning Zhang et al. (2024) approach on few-shot setting as well as recent peer-reviewed weights generation studies Schürholt et al. (2022b); Schürholt et al. (2024).
- Our method enables learning from a distribution of diverse pre-trained models, each trained on different datasets while matching individual pretrained model performance.
- It scales to small and large datasets, generating weights for architectures with over 400 million parameters including GPT2-Small.
- We demonstrate its effectiveness in improving LLM performance by generating task-specific weights from a single pretrained model and our sampled weights based LLAMA3-.1-8B and LLAMA3-.2-1B models ranked among top 2 performing models on the open lm-leaderboard<sup>1</sup>

## 2 RELATED WORK

**Neural Network Parameters Prediction:** As neural networks expand across domains, transfer learning through pretrained weights has become crucial. While hypernetworks have emerged as a promising approach for weight prediction (Chauhan et al., 2023; Ratzlaff & Fuxin, 2020; Denil

<sup>1</sup>[https://huggingface.co/spaces/open-llm-leaderboard/open\\_llm\\_leaderboard](https://huggingface.co/spaces/open-llm-leaderboard/open_llm_leaderboard)

et al., 2013; Ha et al., 2016), subsequent Graph Hypernetworks (GHN) methods leverage model architecture graphs to generate weights (Zhang et al., 2019; Knyazev et al., 2021; Zhmoginov et al., 2022; Knyazev et al., 2023). Though recent transformer-based approaches treat weight generation as an autoregressive process (Zhmoginov et al., 2022), these methods remain constrained by their single-task focus, limiting their transfer learning capabilities. Similar to GHNs diffusion models has been used to generate weights in meta learning setting Nava et al. (2023); Zhang et al. (2024) However, the generated parameters are not task-specific and the generator was limited to classifier head.

**Parameters Generation from Pretrained Distribution:** Parameter generation from pretrained distributions has emerged as a promising research direction due to its practical applications. However, existing approaches (Schürholt et al., 2021; Schürholt et al., 2022a; Peebles et al., 2022; Schürholt et al., 2024) remain constrained by their focus on single-dataset parameter learning, leaving the broader potential of cross-domain applications largely unexplored.

**Applications of Parameter Generation in LLMs:** Despite skepticism around learning from pretrained weight distributions, our approach generates diverse task-specific weights for LLMs (Minace et al., 2024; Zhao et al., 2023; Dubey et al., 2024). By generating specialized LoRA modules (Tang et al., 2024; Zhao et al., 2024; Gong et al., 2024), we can enhance model flexibility and transfer learning while reducing computational costs.

### 3 APPROACH

#### 3.1 PRELIMINARY

Consider a collection of neural network models  $\{\mathcal{A}_i\}_{i=1}^M$ , each pretrained on one of  $M$  distinct datasets  $\{\mathcal{D}_1, \mathcal{D}_2, \dots, \mathcal{D}_M\}$ . Our primary objective is to characterize and learn the underlying distribution  $p(W)$  of the pretrained model weights  $W$  across this ensemble. The ultimate goal is to develop a method for conditional sampling of weights  $p(W_T|\mathcal{D}_T)$  that are optimized for any target dataset or task  $\mathcal{D}_T(x, y)$ , regardless of whether it appeared in the training collection. These sampled weights should either achieve strong performance on  $\mathcal{D}_T$  immediately (or require minimal fine-tuning compared to random initialization). The intuition is that there is a direct relationship between a pretrained network weights and the dataset it was trained on (see Appendix A.1 for a formal argument). We argue that this relationship constrains the high-dimensional weight space  $\mathcal{W} \in \mathbb{R}^n$  to a lower-dimensional manifold  $\mathcal{M} \subset \mathcal{W}$  with dimension  $k \ll n$ . This hypothesis is supported by the Lottery Ticket literature (Frankle & Carbin, 2019; Liu et al., 2024), which shows that sparse subnetworks can match full network performance:  $\mathcal{L}(\theta; \mathcal{D}) \approx \mathcal{L}(\theta \odot m; \mathcal{D})$ , where  $m \in \{0, 1\}^n$  is a sparse mask. By Whitney’s Embedding Theorem (Whitney, 1936),  $\mathcal{M}$  can be smoothly embedded in  $\mathbb{R}^{2k+1}$  via a diffeomorphism  $\phi: \mathcal{M} \rightarrow \mathcal{Z}$ , where  $\mathcal{Z}$  represents a latent space. We approximate this embedding using a variational autoencoder (VAE). Given the differentiability of  $\mathcal{Z}$ , we can employ latent diffusion to model the distribution of pretrained weights. This enables our proposed D2WNG framework to not only preserve individual model performance but also generalize to unseen datasets as we incorporate more pretrained models, leveraging the smoothness and interpolation properties of the latent space. Later, we investigate some possible way to improve LLMs without fine-tuning through optimal weights latent space exploration via sampling with D2NWG. In this paper, we use the terms *seen dataset/task* and *unseen dataset/task* to refer to datasets or tasks that are present in or absent from the training set, respectively and Zero-shot means not optimization step just inference.

#### 3.2 WEIGHT ENCODING

Let  $\{\mathcal{M}_i\}_{i=1}^N$  be a set of pretrained models. For each  $\mathcal{M}_i$ , we flatten its weights to  $W_i \in \mathbb{R}^{d_i}$  where  $d_i$  is its parameter count. Define  $d_{\max} = \max_i d_i$ . We zero-pad each  $W_i$  to obtain  $\hat{W}_i \in \mathbb{R}^{d_{\max}}$ , giving uniform-length representations (Figure 1) to which we refer to as model-wise vectorization. This setting is suitable for small models and classifier layer adaptation. On the other hand, Layer-wise vectorization keeps each layer’s weights separate rather than concatenating them. Each flattened weight vector  $w \in \mathbb{R}^{mn}$  is zero-padded to match a chosen chunk size multiple, then split into  $k$  equal-length subvectors  $\bar{w}_i \in \mathbb{R}^l$  where  $l = \lceil mn/k \rceil$ . This enables independent layer-wise sampling during inference, where each vectorized layer serves as a separate input for subsequent stages. This setting is suitable for large models.

**Params Encoding:** We then train a Variational Autoencoder (VAE) to encode these vectors. while minimizing the objective function defined in 1:

$$\mathcal{L} = -\mathbb{E}_{q_\phi(z|w)} [\log p_\theta(w|z)] + \beta \text{KL} [q_\phi(z|x) || p(z)] \quad (1)$$

where  $w$  is the vectorized weight,  $z$  is the latent representation,  $p_\theta$  and  $q_\phi$  the reconstruction and approximate posterior terms respectively, and  $p(z)$  the prior distribution. For the prior, we used a Gaussian.  $\beta$  is a fixed hyper parameters that regulate the stochasticity of the VAE. Higher value increase the randomness while lower value increases the reconstruction precision with less randomness. Model-wise and layer-wise vectorized parameters are encoded using the same VAE structure, with the only difference being in the input dimensions. In chunk-wise encoding, the original flattened vector  $w$  is recovered by reassembling the decoded latent chunks through concatenation. The reconstructed chunks  $\hat{w}_i$  from each layer are concatenated to ensure  $\hat{w} = \hat{w}_1 \oplus \hat{w}_2 \oplus \dots \oplus \hat{w}_k$ , where  $\oplus$  denotes concatenation. And reshaping  $\hat{w}$  back into the original form  $\hat{W}$  yields a close approximation of the original weight  $W$ . The quality of reconstruction is assessed by evaluating the reconstructed weights on a designated evaluation dataset or task.

### 3.3 DATASET ENCODING

**Image Dataset Encoding:** We adopt a Set Transformer-based encoder (Lee et al., 2019a)  $\mathcal{T}$  to encode the pretraining datasets. This approach effectively handles large, multi-class datasets and has been validated in prior dataset-adaptive methods (Jeong et al., 2021; Lee et al., 2021). Figure 5 in the appendix provides an architectural overview of the dataset encoder. Given a dataset with  $C$  classes denoted by  $\mathcal{D} = \{(x_i, y_i)\}_{i=1}^C$ , where  $x_i$ , and  $y_i$  denote inputs and labels, we use pretrained clip image encoder to extract the images features and group the data into subsets  $s_i$  by class, forming  $\mathcal{S} = \{s_i\}_{i=1}^C$  with  $s_i \in \mathbb{R}^{C \times K_i \times d_{feat}}$ . Here  $K_i$  is the number of images belonging to class  $i$ , and  $d_{feat}$  the features dimension. Each subset is transformed into embeddings  $z_{s_i} \in \mathbb{R}^{1 \times d}$  using a transformation  $\mathcal{T}$ , and these embeddings are aggregated into  $\tilde{s}_i \in \mathbb{R}^{C \times d}$ . Another transformation  $\mathcal{T}$  produces the final dataset encoding  $z_{\mathcal{D}} \in \mathbb{R}^d$ , represented as:  $z_{\mathcal{D}} = \mathcal{T} \circ \mathcal{T}(\mathcal{S})$  This encoding is invariant to the number of classes and dataset size, and it operates without utilizing labels. We train the dataset encoder  $\mathcal{T}$  using a contrastive loss to align dataset embeddings  $z_{\mathcal{D}_i}$  with pretrained weight embeddings  $z_i$ , following the CLIP-style approach introduced in HyperCLIP (Nava et al., 2023). This alignment ensures training stability and computational efficiency during diffusion optimization.

$$\mathcal{L}_{\text{CLIP}} = -\log \frac{\exp(z_i \cdot z_{\mathcal{D}_i} / \tau)}{\sum_{k=1}^N \exp(z_i \cdot z_{\mathcal{D}_k} / \tau)}, \quad (2)$$

where  $z_{\mathcal{D}_i}$  is the dataset embedding for  $\mathcal{D}_i$ , and  $z_i$  is the corresponding VAE-encoded weight embedding (see Section 3.2). This alignment enables efficient probing and integration into downstream tasks.

**Language Task Encoding:** To enable task-description-based parameter generation for NLP tasks, we first encode each task description using Llama-3-8B-Instruct. The output from the last hidden layer is used as the task’s dataset embedding. These embeddings are then directly incorporated into the diffusion process during both training and inference.

### 3.4 DATASET-CONDITIONED PARAMETERS GENERATION

At this stage, we have access to a pretrained VAE for encoding neural network weights and a pretrained Set Transformer module to encode entire datasets. The next stage involves defining a model to generate latent representations of weights conditioned on the dataset embeddings. We achieve this by using diffusion probabilistic models (DDPM) (Ho et al., 2020a; Rombach et al., 2021) trained on the latent representation of the pretrained weights..

**Forward Process:** Given a weight embedding  $z$ , obtained from the encoder of the pretrained VAE, the forward diffusion process involves successive Gaussian noise perturbations of  $z$  over  $T$  time steps. At time step  $t$ ,

$$p(z_t | z_{t-1}) = \mathcal{N}(z_t; \mu_t = \sqrt{1 - \beta_t} z_{t-1}, \beta_t I) \quad (3)$$

where  $\beta_t \in (0, 1)$  is the noise variance and  $p(z_{1:T} | z_0) = \prod_{i=1}^T p(z_i | z_{i-1})$ .

**Reverse Process:** As in most DDPM approaches the reverse process is approximated by a neural network such that:

$$p_{\theta}(z_{t-1}|z_t) = \mathcal{N}(z_{t-1}; \mu_{\theta}(z_t, t), \Sigma_{\theta}(z_t, t)), \quad (4)$$

where  $\mu_{\theta}$  and  $\Sigma_{\theta}$  are neural networks.

**Dataset-Conditioned Training:** The diffusion model is trained on the VAE embeddings  $z$ , conditioned on the dataset embeddings concatenated with the latent representations of the weights. To leverage existing architectures, we designed the VAE to generate latent representations that are compatible with standard latent diffusion models with minimal adjustments, optimizing the latent diffusion objective defined in Eq. 5.

$$\mathcal{L}_{LDM} = \mathbb{E}_{z, \varepsilon \sim \mathcal{N}(0,1), Z_{\mathcal{D}}, t} [\|\varepsilon - \varepsilon_{\psi}(z_t, z_{\mathcal{D}}, t)\|_2^2], \quad (5)$$

where  $\varepsilon_{\psi}(z_t, z_{\mathcal{D}}, t)$  is implemented as a UNet.

**Sampling:** New weights are sampled conditionally through the reverse diffusion process as follows:

$$z_t = \frac{1}{\sqrt{a_t}} \left( z_t - \frac{\beta_t}{\sqrt{1-a_t}} \varepsilon_{\psi}(z_t, z_{\mathcal{D}}, t) \right) + \sigma \xi, \quad (6)$$

where  $\xi \sim \mathcal{N}(0, I)$  and,  $\sigma_t$  a chosen value. After sampling a latent representation ( $\bar{z}$  for a given dataset  $\mathcal{D}_i$ ). The pretrained VAE decoder is used to transform these latents into a weight vector  $\bar{w} = \mathcal{D}(\bar{z})$ , which is then used to initialize the target network as shown in Figure 1.

### 3.5 EXPLORING THE OPTIMAL PARAMETERS SPACE OF LLMs

In this section, we extend our method to enhance pretrained LLM performance without fine-tuning by recasting D2NWG as a layer-conditioned parameter generation approach. The key challenge is managing the vast parameter space of LLMs. Drawing from (Hartford et al., 2024), we use the Marchenko-Pastur distribution to identify crucial layers for improving the performance base on weights spectrum. We calculate a signal-to-noise ratio (SNR) to distinguish significant weights from noise as:  $SNR = \frac{\sum_k |\sigma_k| \geq \varepsilon \sigma_k}{\sum_n |\sigma_n| < \varepsilon \sigma_n}$ , where eigenvalues  $\sigma_n$  above threshold  $\varepsilon$  represent meaningful signals, while those below are considered noise. In this section we employ layer-wise chunking to manage large layer. We provide more detailed in the appendix in A.3 and A. Additionally, we present a sequential optimal space exploration algorithm, detailed in ALG. 1.

## 4 EXPERIMENTS

We evaluate our method both with and without finetuning on Few-Shot Learning, Zero-Shot Learning (no fine-tuning), and Model Retrieval tasks. All experiments use a single Titan RTX GPU except experiment with LLMs which used a single A100-80Gb. Detailed ablation studies are provided in the Appendix An extensive set of ablation studies on the proposed method is provided in Appendix C and E

### 4.1 WEIGHT GENERATION WITHOUT FINETUNING ON UNSEEN TASK

We present a set of results where the generated weights are evaluated directly without finetuning for few-shot learning and transferring for unseen Tasks.

#### 4.1.1 WEIGHTS GENERATION FOR FEW-SHOT LEARNING

**Task:** We aim to show that learning the distributions of model pretrained independently on a large set of dataset can enable sampling weights that compete with meta-learning techniques in multi-task few-shot learning, without requiring fine-tuning.

**Dataset:** We utilize the *mini*-ImageNet and *tiered*-ImageNet datasets for this task. For the architectures, we use a four-layer ConvNet and a ResNet12 backbone provided by Chen et al. (2021). We generate the pretrained weights by linear probing a classifier head on each of the 50,000 subsets for 10 epochs and evaluate the performance on 600 subsets from the unseen test split for 1-shot and 5-shot. Analogously to few shot learning, we choose the number of images per class for conditioning

Table 1: Few-Shot Learning. ALL implies generation of the entire parameters and CH denotes generation of classification head only.

Method	Adaptation	Backbone	mini-ImageNet		tiered-ImageNet	
			5-way 1-shot	5-way 5-shot	5-way 1-shot	5-way 5-shot
iMAML (Rajeswaran et al., 2019)	ALL	Conv4	49.30 ± 1.88%	59.77 ± 0.73%	38.54 ± 1.37%	60.24 ± 0.76%
ALFA (Baik et al., 2020)	ALL	Conv4	50.58 ± 0.51%	69.12 ± 0.47%	53.16 ± 0.49%	70.54 ± 0.46%
COMLN (Deleu et al., 2022)	CH	Conv4	53.01 ± 0.62%	70.54 ± 0.54%	54.30 ± 0.69%	71.35 ± 0.57%
MetaQDA (Zhang et al., 2021)	CH	Conv4	56.41 ± 0.80%	72.64 ± 0.62%	58.11 ± 0.48%	74.28 ± 0.73%
MetaDiff (Zhang et al., 2024)	CH	Conv4	55.06 ± 0.81%	73.18 ± 0.64%	57.77 ± 0.90%	75.46 ± 0.69%
D2N WG(Ours)	CH	Conv4	<b>61.13 ± 8.50%</b>	<b>76.94 ± 6.04%</b>	<b>65.33 ± 6.50%</b>	<b>80.05 ± 8.25%</b>
ALFA (Baik et al., 2020)	ALL	ResNet12	59.74 ± 0.49%	77.96 ± 0.41%	64.62 ± 0.49%	82.48 ± 0.38%
MetaOptNet (Lee et al., 2019b)	CH	ResNet12	62.64 ± 0.61%	78.63 ± 0.46%	65.99 ± 0.72%	81.56 ± 0.53%
LEO (Rusu et al., 2019)	CH	WRN-28-10	61.76 ± 0.08%	77.59 ± 0.12%	66.33 ± 0.05%	81.44 ± 0.09%
Classifier (Chen et al., 2021)	CH	ResNet12	61.22 ± 0.84%	78.72 ± 0.60%	69.71 ± 0.88%	83.87 ± 0.64%
MetaQDA (Zhang et al., 2021)	CH	ResNet18	65.12 ± 0.66%	80.98 ± 0.75%	69.97 ± 0.52%	85.51 ± 0.58%
MetaDiff (Zhang et al., 2024)	CH	ResNet12	64.99 ± 0.77%	81.21 ± 0.56%	72.33 ± 0.92%	86.31 ± 0.62%
D2N WG(Ours)	CH	ResNet12	<b>69.55 ± 3.77%</b>	<b>83.51 ± 6.21%</b>	<b>81.15 ± 9.70%</b>	<b>90.04 ± 6.10%</b>

Table 2: Zero-Shot Transfer Learning. We evaluate on two backbones: Tiny Swin Transformer and ResNet18.

Model	CIFAR-10	STL-10	Aircraft	Pets	CIFAR-100
Swin	7.38	8.43	5.01	2.63	1.35
GHN2 (Knyazev et al., 2021)	48.20	-	-	-	12.7
GHN3 (Knyazev et al., 2023)	51.8	-	-	-	11.9
D2N WG(Ours)	<b>53.12 ± 0.25</b>	<b>60.42 ± 0.14</b>	<b>24.57 ± 3.16</b>	<b>26.47 ± 1.90</b>	<b>30.44 ± 0.15</b>
ResNet18	10.88	6.78	3.75	2.39	1.38
GHN2 (Knyazev et al., 2021)	19.52	13.04	-	-	-
D2N WG	33.03 ± 0.04	50.42 ± 0.13	17.60 ± 2.13	17.29 ± 0.13	13.71 ± 0.63
D2N WG_CLIP(Ours)	<b>60.42 ± 0.75</b>	<b>82.42 ± 0.04</b>	<b>27.70 ± 3.24</b>	<b>32.17 ± 6.30</b>	<b>51.50 ± 0.25</b>

to be the same as the support set, while the number of images per class in the query set is fixed to 15 for all methods and 600 tasks are used for testing.

**Baselines:** We benchmark against iMAML (Rajeswaran et al., 2019), ALFA (Baik et al., 2020), COMLN (Deleu et al., 2022), MetaQDA (Zhang et al., 2021), MetaDiff (Zhang et al., 2024), MetaOptNet (Lee et al., 2019b) and a classifier baseline introduced in Chen et al. (2021).

**Results:** Table 1 shows that our approach consistently improves performance on all tasks while utilizing the same backbone as other methods. With the Conv4 backbone, we achieve approximately 6% performance improvement in 1-shot learning and 3 to 4% on 5-shot learning on mini-ImageNet. On Tiered-ImageNet, we achieve more than 8% performance improvement on 1-shot and 5 to 6% average improvement on 5-shots. For the ResNet12 backbone we achieve 4 to 9% performance improvement. These results demonstrate the effectiveness of our method against the existing meta-learning methods.

For evaluation, we perform 50 weight sampling iterations per subset and report the average of the top 3 accuracies. We explore both 1-shot and 5-shot settings, using one and five images per class respectively for conditioning from support set. Our dataset-conditioned weight generation enables efficient task adaptation by producing weights specialized to each dataset’s characteristics, achieving superior generalization compared to meta-learning baselines.

#### 4.1.2 ZERO-SHOT CLASSIFIER HEAD ADAPTATION

**Task:** We evaluate the performance of the proposed method in adapting the classifier head to unseen datasets. In this experiment, we assess whether our method can conditionally generate the classifier weights, potentially eliminating or significantly speeding up the finetuning process.

**Dataset:** We partitioned ImageNet-1k into 20k subsets of 50 classes each with 50 images per class per subset and linear probe a classifier head for 10 epochs using Tiny Swin Transformer (denoted Swin in Table 1), and ResNet18 all pretrained on ImageNet-1k. For dataset conditioning, we use 5 images per class per subset. The unseen target datasets are CIFAR-10, STL-10, Aircraft, Pets, and

Table 3: Model Retrieval via Generative Augmented Weight Sampling

Domain	Pretrained	D2N WG(Ours)
Large Animals	71.11 ± 11.45	70.33 ± 12.42
Small Animals	54.04 ± 13.56	54.70 ± 13.83
Plants	63.69 ± 9.05	71.37 ± 17.15
Plant Diseases	81.69 ± 19.14	81.98 ± 19.53
Microscopy	55.56 ± 26.14	55.49 ± 26.17
Remote Sensing	82.20 ± 7.49	82.68 ± 8.05
Vehicles	57.07 ± 19.57	58.09 ± 18.30
Manufacturing	84.34 ± 21.00	84.32 ± 20.96
Human Actions	68.63 ± 12.45	69.09 ± 12.73
OCR	63.18 ± 1.75	65.60 ± 2.00
Average	68.32 ± 13.84	<b>69.47 ± 14.79</b>
Runtime	6 hours	40 seconds

CIFAR-100 . The baseline methods in these experiments are ResNet18 and Tiny Swin Transformer pretrained on ImageNet-1k.

**Baselines:** We benchmark against the pretrained backbones, and two GHN models (Knyazev et al., 2021; 2023). Additionally, we provide a powerful variant of our model D2NWG\_CLIP where the dataset encoder encodes the CLIP embedding for each sample in the datasets.

**Results:** Table 2 presents the performance of the sampled weights where it can be seen that the proposed method achieves better performance compared to the ImageNet pretrained weights and the GHN family of models. Additionally, the variant of our model that utilizes the CLIP embedding for dataset encoding significantly improves the performance suggesting that better dataset representation learning can boost the performance of the generated weights.

#### 4.1.3 IN DISTRIBUTION FULL MODELS WEIGHTS GENERATION: MODEL RETRIEVAL

**Task:** We assess the Generative Augmented Retrieval capability of D2NWG , aiming to show that it can learn the distribution of models pretrained on diverse real-world datasets. This task requires generation of dataset-conditioned weights that achieve performance comparable to the original pretrained models and hence provide access to a wide range of pretrained models through efficient sampling.

**Dataset:** We collected 30 real-world datasets(Ullah et al., 2022), spanning 19 to 706 classes and organised into 10 domains with 3 datasets per domain, and fine-tuned a MobileNetV3 subnet<sup>2</sup> sampled from OFA (Cai et al., 2020) for 100 epochs on each dataset. We then learned the distribution of the combined pretrained models from the last 20 epochs across all datasets.

**Baselines:** For this task, we compare with the original pretrained weights which are finetuned on each individual dataset. For each dataset, we sample and report the average accuracy of 5 set of weights sampled with D2NWG .

**Results:** From Table 3 we see that D2NWG conditionally generates high-performing parameters while enhancing the pretrained model, achieving the best average results across all datasets. This demonstrates the strong retrieval capability of our method, suggesting it can be used as a neural network weight retriever in approaches like (Zhao et al., 2024), eliminating the need for pretrained database. Detailed dataset information is provided in Table 12 and more experiments in the Appendix C.10. Additionally, it is much more efficient to generate weights with our model compared to pretraining as shown by the runtime in Table 3.

#### 4.1.4 TRANSFERING TO UNSEEN ARCHITECTURE

We investigate weight transferability across ResNet architectures by modeling the distribution of pretrained weights from ResNet32 (trained on CIFAR-10 and CIFAR-100). We propose a weight initialization method that leverages pretrained weight distributions from ResNet32 to improve performance across different ResNet architectures. Our approach samples and concatenates weights from the source model while preserving layer-type correspondence, effectively handling varying network dimensions. Experiments on ResNet20/44/56/32 demonstrate consistent improvements over random initialization, even without fine-tuning, particularly on CIFAR-10 classification tasks

Table 4: Finetuning of Generated Weights using the Modelzoo of Schürholt et al. (2022c).

Epoch	Method	MNIST	SVHN	CIFAR-10	STL
0	RandomInit	~10 %	~10 %	~10 %	~10 %
0	<i>SKDE30</i>	68.6±6.7	54.5±5.9	<i>n/a</i>	<i>n/a</i>
0	<i>SAN E<sub>KDE30</sub></i>	84.8±0.8	70.7±1.4	56.3±0.5	39.2±0.8
0	<i>SAN E<sub>SUB</sub></i>	<b>86.7±0.8</b>	<b>72.3±1.6</b>	57.9±0.2	43.5±1.0
0	D2NWG	80.52±0.82	66.6±0.7	<b>58.80±0.1</b>	<b>44.50±0.1</b>
1	RandomInit	20.6±1.6	19.4±0.6	37.2±1.4	21.3±1.6
1	<i>SKDE30</i>	83.7±1.3	69.9±1.6	<i>n/a</i>	<i>n/a</i>
1	<i>SAN E<sub>KDE30</sub></i>	85.5±0.8	71.3±1.4	58.2±0.2	43.5±0.7
1	<i>SAN E<sub>SUB</sub></i>	87.5±0.6	73.3±1.4	59.1±0.3	44.3±1.0
1	D2NWG	<b>87.8±0.4</b>	<b>73.6±1.3</b>	<b>59.2±0.3</b>	<b>44.8±0.2</b>
5	RandomInit	36.7±5.2	23.5±4.7	48.5±1.0	31.6±4.2
5	<i>SKDE30</i>	92.4±0.7	57.3±12.4	<i>n/a</i>	<i>n/a</i>
5	<i>SAN E<sub>KDE30</sub></i>	87.5±0.7	72.2±1.2	58.8±0.4	45.2±0.6
5	<i>SAN E<sub>SUB</sub></i>	89.0±0.4	73.6±1.5	59.6±0.3	44.3±0.9
5	D2NWG	<b>92.5±0.9</b>	<b>74.0±0.1</b>	<b>60.3±0.1</b>	<b>45.4±0.1</b>
25	RandomInit	83.3±2.6	66.7±8.5	57.2±0.8	44.0±1.0
25	<i>SKDE30</i>	93.0±0.7	74.2±1.4	<i>n/a</i>	<i>n/a</i>
25	<i>SAN E<sub>KDE30</sub></i>	92.0±0.3	74.7±0.8	60.2±0.6	48.4±0.5
25	<i>SAN E<sub>SUB</sub></i>	92.3±0.4	75.1±1.0	61.2±0.1	48.0±0.4
25	D2NWG	<b>96.2±0.3</b>	<b>75.7±0.5</b>	<b>64.1±1.0</b>	<b>48.7±0.5</b>
50	RandomInit	91.1±2.6	70.7±8.8	61.5±0.7	47.4±0.9

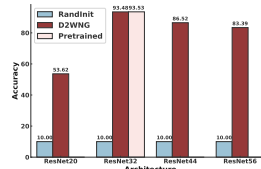


Figure 2: Performance evaluation with unseen architectures on CIFAR-10.

<sup>2</sup>[https://pytorch.org/hub/pytorch\\_vision\\_once\\_for\\_all/](https://pytorch.org/hub/pytorch_vision_once_for_all/)

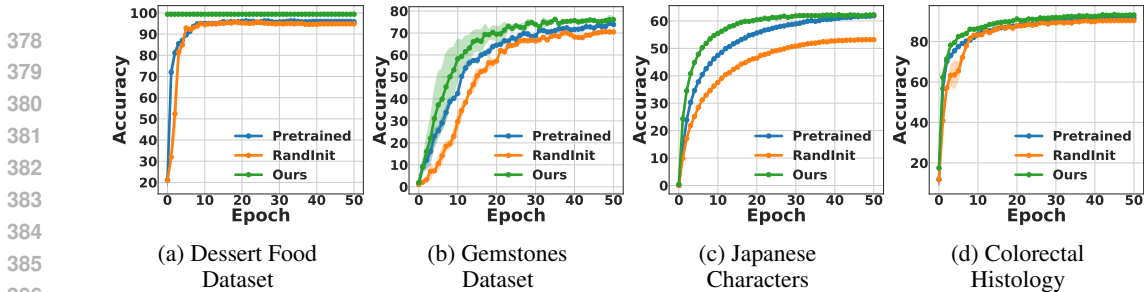


Figure 3: Average accuracy evolution of fine-tuning for 50 epochs with sampled weights for unseen datasets.

## 4.2 WEIFHTS GENERATION WITH FINE-TUNING

In this section, we evaluate the quality of the generated weights in fine-tuning scenarios to assess their suitability for transfer learning.

### 4.2.1 WEIGHT GENERATION WITH FINE-TUNING ON SEEN TASKS

**Task:** The goal is to assess the behavior of the sampled weights when finetuned on the same dataset and compare convergence speed. This experiment focuses on evaluating whether the sampled weights can be effectively fine-tuned to achieved superior final performance, rather than simply aiming for weights producing high initial accuracy and may not lead to superior performance while fine-tuning.

**Datasets:** We used the modelzoo of Schürholt et al. (2022c) consisting of a ConvNet trained on MNIST, SVHN, CIFAR-10 and STL-10. Our model was trained on the combined pretrained weights from epochs 21 to 25 of all models, consistent with the baseline settings.

**Baselines:** We compare against the kernel density estimator approaches from Schürholt et al. (2024); Schürholt et al. (2022b), evaluated on the same datasets. Unlike these unconditional methods, we build a model specifically for MNIST and SVHN, and another for CIFAR-10 and STL-10. For each dataset, five sets of weights were sampled to initialize the models, which were fine-tuned for a number of epochs from 0 to 25. We also add RandomInit model trained for 50 epochs and show that our sampled weight finetuned for 25 epochs outperforms this model.

**Results:** As shown in Table 4, D2NWG consistently accelerates convergence across related tasks, surpassing the pretrained model and outperforming both baselines Schürholt et al. (2022a); Schürholt et al. (2024). The finding implies that D2NWG accelerates convergence and improves performance compared to existing methods. This highlights its potential for faster and more efficient model initialization, making it valuable for transfer learning and real-world applications. Interestingly, on MNIST and SVHN, weights with higher initial performance tend to degrade during fine-tuning.

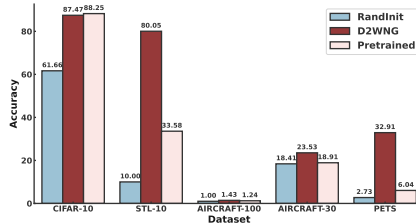


Figure 4: Comparison of accuracy for Pre-trained, D2NWG, and RandInit methods across CIFAR-10, STL-10, Aircraft100, Aircraft30, and Pets after 1 epoch of fine-tuning.

### 4.2.2 FINE-TUNING ON UNSEEN TASKS:MLP CLASSIFIER

**Task:** The objective remains the same as in Section 4.2.1, but here we evaluate the proposed method solely on unseen datasets.

**Datasets:** We assess D2NWG on a real-world dataset of 140 subsets with class counts ranging from 2 to 20, and 10 test sets with up to 1,566 classes. We use a two-layer MLP on top of a CLIP image encoder and fine-tune it on training datasets to collect the pretrained zoo.(see appendix A.5). The image datasets contains food, dataset, drawing, x-ray and others.

**Baselines:** The baseline methods are random initialization and a pretrained MLP previously trained on ImageNet.



**Results:** Figure 3 shows performance on four unseen datasets, where D2NKG achieves 99.04% initial accuracy on the dessert dataset, outperforming the randomly initialized model even after 50 epochs. D2NKG consistently accelerates convergence across all tasks, surpassing both random and pretrained initialization. Despite no class overlap between training and test datasets, it demonstrates strong transferability. Detailed results are available in Table 22 of the Appendix.

#### 4.2.3 FULL MODELS FINE-TUNING ON UNSEEN TASKS

**Task:** We evaluate each method’s generalization on CIFAR-10, STL-10, Pets and Aircrafts, focusing on performance gains in domain-specific tasks. The goal is to identify the best initialization strategy for improving model adaptability across diverse data distributions.

**Baseline:** The baseline in this experiment are the Pretrained model, which uses weights from a model pretrained on ImageNet and RandomInit, a randomly initialized model.

Table 5: Task Conditioned LoRA parameters Generation. Adaptations are performed on a Roberta-Base model denoted Rob-B.

Method	Parameters	SST-2 (Acc)	MRPC (Acc.)	CoLa MCC.)	QNLI (Acc.)	RTE (Acc.)	STS-B (PCC.)	Avg.
Rob-B	125M	<b>94.8</b>	90.2	63.6	<b>92.8</b>	78.7	91.2	85.2
LoRA	0.9M	95.1±0.2	89.7±0.7	63.4±1.2	93.3±0.3	78.4±0.8	91.5±0.2	85.2
AdaLoRA	0.9M	94.5±0.2	88.7±0.5	62.0±0.6	93.1±0.2	81.7±0.6	90.5±0.2	85.0
DyLoRA	0.9M	94.3± 0.5	89.5±0.5	61.1±0.6	92.2±0.1	78.7±0.7	91.1±0.2	84.5
FourierFT	0.6M	94.2±0.3	90.0 ± 0.8	63.8±1.6	92.2±0.1	79.1±0.5	90.80 ± 0.2	85.0
D2NKG	0.6M	94.3±0.1 +0.2	<b>90.3±0.5(†0.3)</b>	<b>64.3±1.2 (†0.5)</b>	92.6±0.2(†0.5)	<b>79.6±0.4(†0.5)</b>	91.0±0.3(†0.0.2)	85.3(†0.3)

**Datasets:** In this experiment we evaluate the transferability to unseen dataset of D2NKG trained in Section 4.1.3 on unseen datasets CIFAR-10, STL-10, Aircraft100, Aircraft30, and Pets.

**Results:** We evaluated D2NKG by comparing it against 5 pretrained and 5 randomly initialized models, each fine-tuned for 1 epoch across CIFAR-10, STL-10, Aircraft100, Aircraft30, and Pets datasets. As shown in Figure 4, D2NKG consistently outperformed the baselines. Notably, on AIRCRAFT-100, D2NKG achieved 1.43% accuracy, surpassing both randomly initialized (1.0%) and ImageNet-pretrained (1.24%) models. These results demonstrate D2NKG’s superior generalization and fine-tuning capabilities, even on specialized datasets.

#### 4.3 TASK CONDITIONED LORA WEIGHTS GENERATION

**Task:** In this section, we demonstrate that our method can be applied to LLMs by learning the distribution of LoRA matrices conditioned on task-specific textual descriptions.

**Datasets:** We use six tasks from the GLUE benchmark and generate task descriptions using GPT-4, as shown in Table 14. LoRA weights were generated following the fine-tuning process of Gao et al. (2024). We collected LoRA and classifier head checkpoints from the last 5 epochs, combined the pretrained vectors, and conditionally learned their distribution.

**Baselines:** We compare with base Roberta-base, LoRA (Hu et al., 2021), AdaLoRA (Zhang et al., 2023), DyLoRA (Valipour et al., 2022) and FourierFT (Gao et al., 2024) which are all LoRA-based RoBERTa-base models. We sampled and compared the average accuracy of the top 5 performing sets of weights per dataset.

**Results:** As shown in Table 5, D2NKG effectively generates weights that match or surpass the performance of pretrained models. These results align with our findings from the augmented weight retrieval experiments. Additional details regarding the task descriptor are provided in Table 14.

#### 4.4 ENHANCING LLM PERFORMANCE WITH WEIGHT SAMPLING

**Task:** We aim to demonstrate that D2NKG can enhance existing LLMs by learning the distribution of their pretrained weights, enabling the generation of parameters that improve performance on specific tasks while generalizing to unseen tasks.

**Datasets:** We evaluate on several benchmarks(Beeching et al., 2023): AI2 Reasoning Challenge for grade-school science questions, HellaSwag for commonsense inference, Winogrande for common-sense reasoning.

Table 7: Performance evaluation on unseen open llms leaderboard v2 benchmark. These results are produced by Huggingface after submission to open LLM leaderboards.  $\uparrow$  indicate performance improvement while  $\downarrow$  indicate a performance decrease

Method	ifeval (0)	Bbh (3)	Gpqa (0)	MATH-hard (4)	Musr (0)	MMLU-Pro (5)	Avg	Base Model	Fine-tuned
Meta-Llama-3.2-1B-Instruct	56.78	8.74	<b>3.36</b>	<b>2.96</b>	<b>2.97</b>	7.58	13.76	Meta-Llama-3.2-1B	No
D2NKG	<b>58.44</b> ( $\uparrow$ 1.66)	<b>8.82</b> ( $\uparrow$ 0.08)	1.68( $\downarrow$ 1.68)	6.04( $\downarrow$ 3.08)	0.66( $\downarrow$ 2.31)	<b>9.09</b> ( $\uparrow$ 1.51)	<b>14.12</b> ( $\uparrow$ 0.36)	Meta-Llama-3.2-8B-Instruct	Yes
SauerkrautLM-8B-Instruct	80.17	31.00	<b>5.37</b>	11.18	11.52	<b>32.12</b>	28.56	Meta-Llama-3.1-8B-Instruct	Yes
D2NKG	<b>80.33</b> +0.16	<b>31.10</b> ( $\uparrow$ 0.10)	5.26( $\downarrow$ 0.11)	<b>11.56</b> ( $\uparrow$ 0.38)	<b>11.52</b>	32.07( $\downarrow$ 0.05)	<b>28.64</b> ( $\uparrow$ 0.08)	SauerkrautLM-8B-Instruct	No
Lexi-Uncensored-V2	77.92	29.69	4.36	16.92	7.77	30.90	27.93	Meta-Llama-3.1-8B-Instruct	Yes
Meta-Llama-3.1-8B-Instruct	<b>78.56</b>	29.89	2.35	<b>17.60</b>	8.41	30.68	27.91	Meta-Llama-3.1-8B	Yes
D2NKG	77.85( $\downarrow$ 0.71)	<b>30.39</b> ( $\uparrow$ 0.5)	<b>4.47</b> ( $\uparrow$ 2.12)	17.52( $\downarrow$ 0.08)	<b>9.64</b> ( $\uparrow$ 1.23)	<b>31.02</b> ( $\uparrow$ 0.34)	<b>28.50</b> ( $\uparrow$ 0.59)	Meta-Llama-3.1-8B-Instruct	No

**Baseline:** We evaluate our method against various version of LLAMA3 and Mistral-7B.

For each model, We extract the weights of the top 25% of layer excluding embedding and output layer, learn their distribution using chunk based encoding, We then steer through the optimal space to generate task-specific parameters as shown in Table 6.

**Results:** The results in Table 6 demonstrates that our approach consistently improve the performance of each models demonstrating new application avenues of our proposed method.

#### 4.5 EVALUATION ON OPEN LM BENCHMARK

We merge these models following Wortsman et al. (2022) and evaluate them on the OpenLM leaderboard (Fourrier et al., 2024) as shown in Table 13

**Task:** We evaluate the robustness of our best models on the open-lm leaderboard.

**Datasets:** We evaluate models on 6 key benchmarks datasets: IFEval for instruction adherence, BBH (Big Bench Hard, with 23 challenging tasks (arithmetic, reasoning, language understanding), MATH focusing on Level 5 high-school math problems, GPQA with graduate-level Q&A across various fields, MuSR testing complex reasoning with long-range context, and MMLU-Pro for advanced multitask knowledge assessment. These benchmarks assess diverse reasoning and knowledge capabilities in and few-shot settings.

**Baselines:** We compare our method against LLAMA3.1-8B-Instruct and its fine-tuned variant, with evaluations conducted on the leaderboard server.

**Results:** As shown in Table 7, our method surpasses baseline models on the leaderboard and performs comparably to models pretrained on task-specific datasets. Despite not being directly calibrated for leaderboard tasks, D2NKG achieves up to a 3% improvement in certain cases. This demonstrates the potential of guided parameter space exploration for task specialization. The consistent gains across benchmarks highlight D2NKG’s effectiveness in enhancing model robustness and transferability, with our LLaMA-3.2-1B model ranking among the top LLaMA-3.2-1B entries on the public leaderboard.

**Quality Check:** Our method enhances text generation quality, as shown in Table 13 Additional results in Appendix D show that the method effectively learns GPT-2 small’s full parameters while maintaining performance comparable to the pretrained model.

## 5 CONCLUSION

In this work, we recast latent diffusion for dataset-conditioned neural network weight generation, enabling quick adaptation to novel datasets and efficient fine-tuning and transfer learning without training. Through extensive experiments on diverse datasets, our method generates high-quality weights for novel tasks and improves generalization. We extend parameter generation to large language models, demonstrating the scalability and versatility of our approach. Our method effectively encodes architectures with up to 1 billion parameters using a single GPU with less than 80GB, including task- or dataset-conditioned generation.

Table 6: Exploration of optimal weight space of some instruct LLMs using a diffusion model sampled weights.  $\uparrow$  indicates the performance gain

Methods	Winogrande (5 shot)	Arc-Challenge (25 shot)	Hellaswag (25 shot)
LLAMA-3.1-8B-Instruct	67.17 $\pm$ 0.01	64.93 $\pm$ 0.01	78.58 $\pm$ 0.00
D2NKG	67.61 $\pm$ 0.02( $\uparrow$ 0.44)	65.74 $\pm$ 0.01( $\uparrow$ 0.81)	78.86 $\pm$ 0.02( $\uparrow$ 0.28)
Mistral-7b-Instruct	69.93 $\pm$ 0.01	59.22 $\pm$ 0.01	81.97 $\pm$ 0.00
D2NKG	70.80 $\pm$ 0.02( $\uparrow$ 0.80)	59.80 $\pm$ 0.01( $\uparrow$ 0.58)	82.04 $\pm$ 0.00( $\uparrow$ 0.07)
LLAMA-3.2-1B-Instruct	56.75 $\pm$ 0.01	40.96 $\pm$ 0.01	61.67 $\pm$ 0.00
D2NKG	57.17 $\pm$ 0.01( $\uparrow$ 0.42)	41.55 $\pm$ 0.01( $\uparrow$ 0.59)	61.70 $\pm$ 0.01( $\uparrow$ 0.03)

## 6 LIMITATION AND ETHICAL STATEMENT

**Limitations:** Our method relies on large collections of pretrained weight tensors and datasets, which require substantial storage and computational resources. However, such pretrained models are becoming more readily available due to the efforts made by open-source communities.

## REFERENCES

- Sungyong Baik, Myungsub Choi, Janghoon Choi, Heewon Kim, and Kyoung Mu Lee. Meta-learning with adaptive hyperparameters. In H. Larochelle, M. Ranzato, R. Hadsell, M.F. Balcan, and H. Lin (eds.), *Advances in Neural Information Processing Systems*, volume 33, pp. 20755–20765. Curran Associates, Inc., 2020.
- Edward Beeching, Clémentine Fourier, Nathan Habib, Sheon Han, Nathan Lambert, Nazneen Rajani, Omar Sanseviero, Lewis Tunstall, and Thomas Wolf. Open llm leaderboard, 2023.
- Han Cai, Chuang Gan, Tianzhe Wang, Zhekai Zhang, and Song Han. Once for all: Train one network and specialize it for efficient deployment. In *International Conference on Learning Representations*, 2020.
- Vinod Kumar Chauhan, Jiandong Zhou, Ping Lu, Soheila Molaei, and David A. Clifton. A brief review of hypernetworks in deep learning. *ArXiv*, abs/2306.06955, 2023. URL <https://api.semanticscholar.org/CorpusID:259138728>.
- Yinbo Chen, Zhuang Liu, Huijuan Xu, Trevor Darrell, and Xiaolong Wang. Meta-baseline: Exploring simple meta-learning for few-shot learning. In *Proceedings of the IEEE/CVF International Conference on Computer Vision*, pp. 9062–9071, 2021.
- Tristan Deleu, David Kanaa, Leo Feng, Giancarlo Kerg, Yoshua Bengio, Guillaume Lajoie, and Pierre-Luc Bacon. Continuous-Time Meta-Learning with Forward Mode Differentiation. In *Tenth International Conference on Learning Representations*, 2022.
- Misha Denil, Babak Shakibi, Laurent Dinh, Marc' Aurelio Ranzato, and Nando de Freitas. Predicting parameters in deep learning. In *Advances in Neural Information Processing Systems*, volume 26. Curran Associates, Inc., 2013.
- Ashwini Doke and Madhava Gaikwad. Survey on automated machine learning (automl) and meta learning. In *2021 12th International Conference on Computing Communication and Networking Technologies (ICCCNT)*, pp. 1–5, 2021. doi: 10.1109/ICCCNT51525.2021.9579526.
- Abhimanyu Dubey, Abhinav Jauhri, Abhinav Pandey, Abhishek Kadian, Ahmad Al-Dahle, Aiesha Letman, Akhil Mathur, Alan Schelten, Amy Yang, Angela Fan, Anirudh Goyal, Anthony Hartshorn, Aobo Yang, Archi Mitra, Archie Sravankumar, Artem Korenev, Arthur Hinsvark, Arun Rao, Aston Zhang, Aurelien Rodriguez, Austen Gregerson, Ava Spataru, Baptiste Roziere, Bethany Biron, Binh Tang, Bobbie Chern, Charlotte Caucheteux, Chaya Nayak, Chloe Bi, Chris Marra, Chris McConnell, Christian Keller, Christophe Touret, Chunyang Wu, Corinne Wong, Cristian Canton Ferrer, Cyrus Nikolaidis, Damien Allonsius, Daniel Song, Danielle Pintz, Danny Livshits, David Esiobu, Dhruv Choudhary, Dhruv Mahajan, Diego Garcia-Olano, Diego Perino, Dieuwke Hupkes, Egor Lakomkin, Ehab AlBadawy, Elina Lobanova, Emily Dinan, Eric Michael Smith, Filip Radenovic, Frank Zhang, Gabriel Synnaeve, Gabrielle Lee, Georgia Lewis Anderson, Graeme Nail, Gregoire Mialon, Guan Pang, Guillem Cucurell, Hailey Nguyen, Hannah Korevaar, Hu Xu, Hugo Touvron, Iliyan Zarov, Imanol Arrieta Ibarra, Isabel Kloumann, Ishan Misra, Ivan Evtimov, Jade Copet, Jaewon Lee, Jan Geffert, Jana Vranes, Jason Park, Jay Mahadeokar, Jeet Shah, Jelmer van der Linde, Jennifer Billock, Jenny Hong, Jenya Lee, Jeremy Fu, Jianfeng Chi, Jianyu Huang, Jiawen Liu, Jie Wang, Jiecao Yu, Joanna Bitton, Joe Spisak, Jongsoo Park, Joseph Rocca, Joshua Johnstun, Joshua Saxe, Junteng Jia, Kalyan Vasuden Alwala, Kartikeya Upasani, Kate Plawiak, Ke Li, Kenneth Heafield, Kevin Stone, Khalid El-Arini, Krithika Iyer, Kshitiz Malik, Kuenley Chiu, Kunal Bhalla, Lauren Rantala-Yeary, Laurens van der Maaten, Lawrence Chen, Liang Tan, Liz Jenkins, Louis Martin, Lovish Madaan, Lubo Malo, Lukas Blecher, Lukas Landzaat, Luke de Oliveira, Madeline Muzzi, Mahesh Pasupuleti, Mannat Singh, Manohar Paluri, Marcin Kardas, Mathew Oldham, Mathieu Rita, Maya Pavlova, Melanie Kambadur, Mike Lewis, Min Si, Mitesh Kumar Singh, Mona

594 Hassan, Naman Goyal, Narjes Torabi, Nikolay Bashlykov, Nikolay Bogoychev, Niladri Chatterji,  
595 Olivier Duchenne, Onur Çelebi, Patrick Alrassy, Pengchuan Zhang, Pengwei Li, Petar Vasic,  
596 Peter Weng, Prajjwal Bhargava, Pratik Dubal, Praveen Krishnan, Punit Singh Koura, Puxin Xu,  
597 Qing He, Qingxiao Dong, Ragavan Srinivasan, Raj Ganapathy, Ramon Calderer, Ricardo Silveira  
598 Cabral, Robert Stojnic, Roberta Raileanu, Rohit Girdhar, Rohit Patel, Romain Sauvestre, Ronnie  
599 Polidoro, Roshan Sumbaly, Ross Taylor, Ruan Silva, Rui Hou, Rui Wang, Saghar Hosseini, Sahana  
600 Chennabasappa, Sanjay Singh, Sean Bell, Seohyun Sonia Kim, Sergey Edunov, Shaoliang Nie,  
601 Sharan Narang, Sharath Rapparth, Sheng Shen, Shengye Wan, Shruti Bhosale, Shun Zhang, Simon  
602 Vandenhennde, Soumya Batra, Spencer Whitman, Sten Sootla, Stephane Collot, Suchin Gururangan,  
603 Sydney Borodinsky, Tamar Herman, Tara Fowler, Tarek Sheasha, Thomas Georgiou, Thomas  
604 Scialom, Tobias Speckbacher, Todor Mihaylov, Tong Xiao, Ujjwal Karn, Vedanuj Goswami,  
605 Vibhor Gupta, Vignesh Ramanathan, Viktor Kerkez, Vincent Gonguet, Virginie Do, Vish Vogeti,  
606 Vladan Petrovic, Weiwei Chu, Wenhan Xiong, Wenyin Fu, Whitney Meers, Xavier Martinet,  
607 Xiaodong Wang, Xiaoqing Ellen Tan, Xinfeng Xie, Xuchao Jia, Xuwei Wang, Yaelle Goldschlag,  
608 Yashesh Gaur, Yasmine Babaei, Yi Wen, Yiwen Song, Yuchen Zhang, Yue Li, Yuning Mao,  
609 Zacharie Delpierre Coudert, Zheng Yan, Zhengxing Chen, Zoe Papakipos, Aaditya Singh, Aaron  
610 Grattafori, Abha Jain, Adam Kelsey, Adam Shajnfeld, Adithya Gangidi, Adolfo Victoria, Ahuva  
611 Goldstand, Ajay Menon, Ajay Sharma, Alex Boesenberg, Alex Vaughan, Alexei Baevski, Allie  
612 Feinstein, Amanda Kallet, Amit Sangani, Anam Yunus, Andrei Lupu, Andres Alvarado, Andrew  
613 Caples, Andrew Gu, Andrew Ho, Andrew Poulton, Andrew Ryan, Ankit Ramchandani, Annie  
614 Franco, Aparajita Saraf, Arkabandhu Chowdhury, Ashley Gabriel, Ashwin Bharambe, Assaf  
615 Eisenman, Azadeh Yazdan, Beau James, Ben Maurer, Benjamin Leonhardi, Bernie Huang, Beth  
616 Loyd, Beto De Paola, Bhargavi Paranjape, Bing Liu, Bo Wu, Boyu Ni, Braden Hancock, Bram  
617 Wasti, Brandon Spence, Brani Stojkovic, Brian Gamido, Britt Montalvo, Carl Parker, Carly Burton,  
618 Catalina Mejia, Changhan Wang, Changkyu Kim, Chao Zhou, Chester Hu, Ching-Hsiang Chu,  
619 Chris Cai, Chris Tindal, Christoph Feichtenhofer, Damon Civin, Dana Beaty, Daniel Kreymer,  
620 Daniel Li, Danny Wyatt, David Adkins, David Xu, Davide Testuggine, Delia David, Devi Parikh,  
621 Diana Liskovich, Didem Foss, Dingkan Wang, Duc Le, Dustin Holland, Edward Dowling, Eissa  
622 Jamil, Elaine Montgomery, Eleonora Presani, Emily Hahn, Emily Wood, Erik Brinkman, Esteban  
623 Arcaute, Evan Dunbar, Evan Smothers, Fei Sun, Felix Kreuk, Feng Tian, Firat Ozgenel, Francesco  
624 Caggioni, Franciso Guzmán, Frank Kanayet, Frank Seide, Gabriela Medina Florez, Gabriella  
625 Schwarz, Gada Badeer, Georgia Swee, Gil Halpern, Govind Thattai, Grant Herman, Grigory Sizov,  
626 Guangyi, Zhang, Guna Lakshminarayanan, Hamid Shojanazeri, Han Zou, Hannah Wang, Hanwen  
627 Zha, Haroun Habeeb, Harrison Rudolph, Helen Suk, Henry Aspegren, Hunter Goldman, Ibrahim  
628 Damlaj, Igor Molybog, Igor Tufanov, Irina-Elena Veliche, Itai Gat, Jake Weissman, James Geboski,  
629 James Kohli, Japhet Asher, Jean-Baptiste Gaya, Jeff Marcus, Jeff Tang, Jennifer Chan, Jenny  
630 Zhen, Jeremy Reizenstein, Jeremy Teboul, Jessica Zhong, Jian Jin, Jingyi Yang, Joe Cummings,  
631 Jon Carvill, Jon Shepard, Jonathan McPhie, Jonathan Torres, Josh Ginsburg, Junjie Wang, Kai  
632 Wu, Kam Hou U, Karan Saxena, Karthik Prasad, Kartikay Khandelwal, Katayoun Zand, Kathy  
633 Matosich, Kaushik Veeraraghavan, Kelly Michelena, Keqian Li, Kun Huang, Kunal Chawla, Kushal  
634 Lakhotia, Kyle Huang, Lailin Chen, Lakshya Garg, Lavender A, Leandro Silva, Lee Bell, Lei  
635 Zhang, Liangpeng Guo, Licheng Yu, Liron Moshkovich, Luca Wehrstedt, Madian Khabza, Manav  
636 Avalani, Manish Bhatt, Maria Tsimpoukelli, Martynas Mankus, Matan Hasson, Matthew Lennie,  
637 Matthias Reso, Maxim Groshev, Maxim Naumov, Maya Lathi, Meghan Keneally, Michael L.  
638 Seltzer, Michal Valko, Michelle Restrepo, Mihir Patel, Mik Vyatskov, Mikayel Samvelyan, Mike  
639 Clark, Mike Macey, Mike Wang, Miquel Jubert Hermoso, Mo Metanat, Mohammad Rastegari,  
640 Munish Bansal, Nandhini Santhanam, Natascha Parks, Natasha White, Navyata Bawa, Nayan  
641 Singhal, Nick Egebo, Nicolas Usunier, Nikolay Pavlovich Laptev, Ning Dong, Ning Zhang,  
642 Norman Cheng, Oleg Chernoguz, Olivia Hart, Omkar Salpekar, Ozlem Kalinli, Parkin Kent, Parth  
643 Parekh, Paul Saab, Pavan Balaji, Pedro Rittner, Philip Bontrager, Pierre Roux, Piotr Dollar, Polina  
644 Zvyagina, Prashant Ratanchandani, Pritish Yuvraj, Qian Liang, Rachad Alao, Rachel Rodriguez,  
645 Rafi Ayub, Raghotham Murthy, Raghu Nayani, Rahul Mitra, Raymond Li, Rebekkah Hogan,  
646 Robin Battey, Rocky Wang, Rohan Maheswari, Russ Howes, Ruty Rinott, Sai Jayesh Bondu,  
647 Samyak Datta, Sara Chugh, Sara Hunt, Sargun Dhillon, Sasha Sidorov, Satadru Pan, Saurabh  
648 Verma, Seiji Yamamoto, Sharadh Ramaswamy, Shaun Lindsay, Shaun Lindsay, Sheng Feng,  
649 Shenghao Lin, Shengxin Cindy Zha, Shiva Shankar, Shuqiang Zhang, Shuqiang Zhang, Sinong  
650 Wang, Sneha Agarwal, Soji Sajuyigbe, Soumith Chintala, Stephanie Max, Stephen Chen, Steve  
651 Kehoe, Steve Satterfield, Sudarshan Govindaprasad, Sumit Gupta, Sungmin Cho, Sunny Virk,  
652 Suraj Subramanian, Sy Choudhury, Sydney Goldman, Tal Remez, Tamar Glaser, Tamara Best,

- 648 Thilo Kohler, Thomas Robinson, Tianhe Li, Tianjun Zhang, Tim Matthews, Timothy Chou, Tzook  
649 Shaked, Varun Vontimitta, Victoria Ajayi, Victoria Montanez, Vijai Mohan, Vinay Satish Kumar,  
650 Vishal Mangla, Vitor Albiero, Vlad Ionescu, Vlad Poenaru, Vlad Tiberiu Mihailescu, Vladimir  
651 Ivanov, Wei Li, Wenchen Wang, Wenwen Jiang, Wes Bouaziz, Will Constable, Xiaocheng Tang,  
652 Xiaofang Wang, Xiaojian Wu, Xiaolan Wang, Xide Xia, Xilun Wu, Xinbo Gao, Yanjun Chen,  
653 Ye Hu, Ye Jia, Ye Qi, Yenda Li, Yilin Zhang, Ying Zhang, Yossi Adi, Youngjin Nam, Yu, Wang,  
654 Yuchen Hao, Yundi Qian, Yuzi He, Zach Rait, Zachary DeVito, Zef Rosnbrick, Zhaoduo Wen,  
655 Zhenyu Yang, and Zhiwei Zhao. The llama 3 herd of models, 2024.
- 656 Clementine Fourier, Nathan Habib, Alina Lozovskaya, Konrad Szafer, and Thomas Wolf. Open llm  
657 leaderboard v2, 2024.
- 658
- 659 Jonathan Frankle and Michael Carbin. The lottery ticket hypothesis: Finding sparse, trainable neural  
660 networks, 2019.
- 661
- 662 Hanan Gani, Muzammal Naseer, and Mohammad Yaqub. How to train vision transformer on small-  
663 scale datasets? In *33rd British Machine Vision Conference 2022, BMVC 2022, London, UK,  
664 November 21-24, 2022*. BMVA Press, 2022.
- 665
- 666 Shanghua Gao, Pan Zhou, Ming-Ming Cheng, and Shuicheng Yan. Masked diffusion transformer  
667 is a strong image synthesizer. In *2023 IEEE/CVF International Conference on Computer Vision  
668 (ICCV)*, pp. 23107–23116, 2023. doi: 10.1109/ICCV51070.2023.02117.
- 669
- 670 Ziqi Gao, Qichao Wang, Aochuan Chen, Zijing Liu, Bingzhe Wu, Liang Chen, and Jia Li. Parameter-  
671 efficient fine-tuning with discrete fourier transform, 2024.
- 672
- 673 Yifan Gong, Zheng Zhan, Yanyu Li, Yerlan Idelbayev, Andrey Zharkov, Kfir Aberman, Sergey  
674 Tulyakov, Yanzhi Wang, and Jian Ren. Efficient training with denoised neural weights, 2024. URL  
675 <https://arxiv.org/abs/2407.11966>.
- 676
- 677 Roberto Gozalo-Brizuela and Eduardo C. Garrido-Merchán. A survey of generative ai applications,  
678 2023.
- 679
- 680 David Ha, Andrew Dai, and Quoc V. Le. Hypernetworks, 2016.
- 681
- 682 Eric Hartford, Lucas Atkins, Fernando Fernandes Neto, and David Golchinfar. Spectrum: Targeted  
683 training on signal to noise ratio, 2024.
- 684
- 685 Jonathan Ho, Ajay Jain, and Pieter Abbeel. Denoising diffusion probabilistic models. In H. Larochelle,  
686 M. Ranzato, R. Hadsell, M.F. Balcan, and H. Lin (eds.), *Advances in Neural Information Processing  
687 Systems*, volume 33, pp. 6840–6851. Curran Associates, Inc., 2020a.
- 688
- 689 Jonathan Ho, Ajay Jain, and Pieter Abbeel. Denoising diffusion probabilistic models. *arXiv preprint  
690 arxiv:2006.11239*, 2020b.
- 691
- 692 Edward J Hu, Yelong Shen, Phillip Wallis, Zeyuan Allen-Zhu, Yanzhi Li, Shean Wang, Lu Wang,  
693 and Weizhu Chen. Lora: Low-rank adaptation of large language models. *arXiv preprint  
694 arXiv:2106.09685*, 2021.
- 695
- 696 Frank Hutter, Lars Kotthoff, and Joaquin Vanschoren (eds.). *Automated Machine Learning - Methods,  
697 Systems, Challenges*. Springer, 2019.
- 698
- 699 Wonyong Jeong, Hayeon Lee, Gun Hong Park, Eunyoung Hyung, Jinheon Baek, and Sung Ju Hwang.  
700 Task-adaptive neural network search with meta-contrastive learning. In *Neural Information  
701 Processing Systems*, 2021.
- 702
- 703 Boris Knyazev, Michal Drozdal, Graham W Taylor, and Adriana Romero-Soriano. Parameter  
704 prediction for unseen deep architectures. In *Advances in Neural Information Processing Systems*,  
705 2021.
- 706
- 707 Boris Knyazev, Doha Hwang, and Simon Lacoste-Julien. Can we scale transformers to predict  
708 parameters of diverse imagenet models? In *International Conference on Machine Learning*, 2023.

- 702 Hayeon Lee, Eunyoung Hyung, and Sung Ju Hwang. Rapid neural architecture search by learning to  
703 generate graphs from datasets. In *International Conference on Learning Representations*, 2021.  
704
- 705 Juho Lee, Yoonho Lee, Jungtaek Kim, Adam Kosior, Seungjin Choi, and Yee Whye Teh. Set trans-  
706 former: A framework for attention-based permutation-invariant neural networks. In *Proceedings*  
707 *of the 36th International Conference on Machine Learning*, pp. 3744–3753, 2019a.
- 708 K. Lee, S. Maji, A. Ravichandran, and S. Soatto. Meta-learning with differentiable convex optimiza-  
709 tion. In *2019 IEEE/CVF Conference on Computer Vision and Pattern Recognition (CVPR)*, pp.  
710 10649–10657, 2019b.  
711
- 712 Bohan Liu, Zijie Zhang, Peixiong He, Zhensen Wang, Yang Xiao, Ruimeng Ye, Yang Zhou, Wei-  
713 Shinn Ku, and Bo Hui. A survey of lottery ticket hypothesis, 2024.  
714
- 715 Shervin Minaee, Tomas Mikolov, Narjes Nikzad, Meysam Chenaghlu, Richard Socher, Xavier  
716 Amatriain, and Jianfeng Gao. Large language models: A survey, 2024. URL <https://arxiv.org/abs/2402.06196>.  
717
- 718 Elvis Nava, Seijin Kobayashi, Yifei Yin, Robert K. Katzschmann, and Benjamin F Grewe. Meta-  
719 learning via classifier(-free) diffusion guidance. *Transactions on Machine Learning Research*,  
720 2023. ISSN 2835-8856.  
721
- 722 William Peebles and Saining Xie. Scalable diffusion models with transformers. In *2023 IEEE/CVF*  
723 *International Conference on Computer Vision (ICCV)*, pp. 4172–4182, 2023. doi: 10.1109/  
724 ICCV51070.2023.00387.
- 725 William Peebles, Ilija Radosavovic, Tim Brooks, Alexei A. Efros, and Jitendra Malik. Learning to  
726 learn with generative models of neural network checkpoints, 2022.  
727
- 728 Aravind Rajeswaran, Chelsea Finn, Sham M Kakade, and Sergey Levine. Meta-learning with implicit  
729 gradients. In H. Wallach, H. Larochelle, A. Beygelzimer, F. d’Alché-Buc, E. Fox, and R. Garnett  
730 (eds.), *Advances in Neural Information Processing Systems*, volume 32. Curran Associates, Inc.,  
731 2019.  
732
- 733 Neale Ratzlaff and Li Fuxin. Hypergan: A generative model for diverse, performant neural networks,  
734 2020.
- 735 R. Rombach, A. Blattmann, D. Lorenz, P. Esser, and B. Ommer. High-resolution image synthesis  
736 with latent diffusion models. In *2022 IEEE/CVF Conference on Computer Vision and Pattern*  
737 *Recognition (CVPR)*, pp. 10674–10685, jun 2022.  
738
- 739 Robin Rombach, A. Blattmann, Dominik Lorenz, Patrick Esser, and Björn Ommer. High-resolution  
740 image synthesis with latent diffusion models. *2022 IEEE/CVF Conference on Computer Vision*  
741 *and Pattern Recognition (CVPR)*, pp. 10674–10685, 2021.
- 742 Andrei A. Rusu, Dushyant Rao, Jakub Sygnowski, Oriol Vinyals, Razvan Pascanu, Simon Osindero,  
743 and Raia Hadsell. Meta-learning with latent embedding optimization. In *International Conference*  
744 *on Learning Representations*, 2019.  
745
- 746 Konstantin Schürholt, Boris Knyazev, Xavier Giró-i Nieto, and Damian Borth. Hyper-representations  
747 as generative models: Sampling unseen neural network weights. In *Thirty-Sixth Conference on*  
748 *Neural Information Processing Systems (NeurIPS)*, September 2022a.
- 749 Konstantin Schürholt, Boris Knyazev, Xavier Giró i Nieto, and Damian Borth. Hyper-representations  
750 as generative models: Sampling unseen neural network weights. In *Advances in Neural Information*  
751 *Processing Systems*, 2022b.  
752
- 753 Konstantin Schürholt, Diyar Taskiran, Boris Knyazev, Xavier Giró-i Nieto, and Damian Borth. Model  
754 zoos: A dataset of diverse populations of neural network models. In *Thirty-Sixth Conference on*  
755 *Neural Information Processing Systems (NeurIPS) Track on Datasets and Benchmarks*, September  
2022c.

- 756 Konstantin Schürholt, Michael W. Mahoney, and Damian Borth. Towards scalable and versatile  
757 weight space learning. In *Proceedings of the 41st International Conference on Machine Learning*  
758 (*ICML*). PMLR, 2024.
- 759  
760 Konstantin Schürholt, Dimche Kostadinov, and Damian Borth. Self-supervised representation learning  
761 on neural network weights for model characteristic prediction. In *Advances in Neural Information*  
762 *Processing Systems (NeurIPS 2021)*, Sydney, Australia, 2021.
- 763  
764 Zihao Tang, Zheqi Lv, Shengyu Zhang, Fei Wu, and Kun Kuang. Modelgpt: Unleashing llm’s  
765 capabilities for tailored model generation, 2024.
- 766  
767 Ihsan Ullah, Dustin Carrion, Sergio Escalera, Isabelle M Guyon, Mike Huisman, Felix Mohr, Jan N  
768 van Rijn, Haozhe Sun, Joaquin Vanschoren, and Phan Anh Vu. Meta-album: Multi-domain  
769 meta-dataset for few-shot image classification. In *Thirty-sixth Conference on Neural Information*  
770 *Processing Systems Datasets and Benchmarks Track*, 2022.
- 771  
772 Mojtaba Valipour, Mehdi Rezagholizadeh, Ivan Kobyzev, and Ali Ghodsi. Dylora: Parameter  
773 efficient tuning of pre-trained models using dynamic search-free low-rank adaptation. *arXiv*  
774 *preprint arXiv:2210.07558*, 2022.
- 775  
776 Kai Wang, Zhaopan Xu, Yukun Zhou, Zelin Zang, Trevor Darrell, Zhuang Liu, and Yang You. Neural  
777 network diffusion, 2024.
- 778  
779 Hassler Whitney. Differentiable manifolds. *Annals of Mathematics*, 37(3):645–680, 1936. doi:  
780 10.2307/1968482.
- 781  
782 Mitchell Wortsman, Gabriel Ilharco, Samir Ya Gadre, Rebecca Roelofs, Raphael Gontijo-Lopes,  
783 Ari S Morcos, Hongseok Namkoong, Ali Farhadi, Yair Carmon, Simon Kornblith, and Ludwig  
784 Schmidt. Model soups: averaging weights of multiple fine-tuned models improves accuracy without  
785 increasing inference time. In Kamalika Chaudhuri, Stefanie Jegelka, Le Song, Csaba Szepesvari,  
786 Gang Niu, and Sivan Sabato (eds.), *Proceedings of the 39th International Conference on Machine*  
787 *Learning*, volume 162 of *Proceedings of Machine Learning Research*, pp. 23965–23998. PMLR,  
788 17–23 Jul 2022.
- 789  
790 Ling Yang, Zhilong Zhang, Yang Song, Shenda Hong, Runsheng Xu, Yue Zhao, Wentao Zhang,  
791 Bin Cui, and Ming-Hsuan Yang. Diffusion models: A comprehensive survey of methods and  
792 applications, 2024. URL <https://arxiv.org/abs/2209.00796>.
- 793  
794 Baoquan Zhang, Chuyao Luo, Demin Yu, Xutao Li, Huiwei Lin, Yunming Ye, and Bowen Zhang.  
795 Metadiff: Meta-learning with conditional diffusion for few-shot learning. *Proceedings of the AAAI*  
796 *Conference on Artificial Intelligence*, 38(15):16687–16695, Mar. 2024.
- 797  
798 Chris Zhang, Mengye Ren, and Raquel Urtasun. Graph hypernetworks for neural architecture search.  
799 In *International Conference on Learning Representations*, 2019.
- 800  
801 Qingru Zhang, Minshuo Chen, Alexander Bukharin, Nikos Karampatziakis, Pengcheng He, Yu Cheng,  
802 Weizhu Chen, and Tuo Zhao. Adalora: Adaptive budget allocation for parameter-efficient fine-  
803 tuning. *arXiv preprint arXiv:2303.10512*, 2023.
- 804  
805 Xueting Zhang, Debin Meng, Henry Gouk, and Timothy Hospedales. Shallow bayesian meta learning  
806 for real-world few-shot recognition. In *2021 IEEE/CVF International Conference on Computer*  
807 *Vision (ICCV)*, pp. 631–640, 2021. doi: 10.1109/ICCV48922.2021.00069.
- 808  
809 Wayne Xin Zhao, Kun Zhou, Junyi Li, Tianyi Tang, Xiaolei Wang, Yupeng Hou, Yingqian Min,  
Beichen Zhang, Junjie Zhang, Zican Dong, Yifan Du, Chen Yang, Yushuo Chen, Zhipeng Chen,  
Jinhao Jiang, Ruiyang Ren, Yifan Li, Xinyu Tang, Zikang Liu, Peiyu Liu, Jian-Yun Nie, and  
Ji-Rong Wen. A survey of large language models, 2023. URL <https://arxiv.org/abs/2303.18223>.
- Ziyu Zhao, Leilei Gan, Guoyin Wang, Yuwei Hu, Tao Shen, Hongxia Yang, Kun Kuang, and Fei Wu.  
Retrieval-augmented mixture of lora experts for uploadable machine learning, 2024.

810 Andrey Zhmoginov, Mark Sandler, and Maksym Vladymyrov. HyperTransformer: Model gener-  
811 ation for supervised and semi-supervised few-shot learning. In Kamalika Chaudhuri, Stefanie  
812 Jegelka, Le Song, Csaba Szepesvari, Gang Niu, and Sivan Sabato (eds.), *Proceedings of the 39th*  
813 *International Conference on Machine Learning*, volume 162 of *Proceedings of Machine Learning*  
814 *Research*, pp. 27075–27098. PMLR, 17–23 Jul 2022.

815  
816  
817  
818  
819  
820  
821  
822  
823  
824  
825  
826  
827  
828  
829  
830  
831  
832  
833  
834  
835  
836  
837  
838  
839  
840  
841  
842  
843  
844  
845  
846  
847  
848  
849  
850  
851  
852  
853  
854  
855  
856  
857  
858  
859  
860  
861  
862  
863



## A APPROACH

**Broader Impact** D2NWDG addresses the resource-intensive nature of deep learning by proposing a method for efficient transfer learning. This has the potential to reduce the computational resources required for training neural networks, making it more accessible to a wider range of researchers and organizations.

**Limitation** In this work, we focus mainly on generalization across datasets. Additionally, while the diffusion model achieves impressive performance on image generation, there are still some challenges to efficiently recast it for weights generation including memory constraint, convergence challenges and considerations of symmetries in the weight spaces of different neural network architectures.

### A.1 RELATIONSHIP BETWEEN DATASETS AND TRAINED WEIGHTS

Gradient descent based optimization is the commonly used technique to generate optimal neural network weights through training by minimizing a loss function, ie. cross-entropy for classification tasks. The weights optimized with gradient descent thus contains some information about the training data. Therefore, understanding the correlation between the training dataset and the optimal weights is important for the generation of weights. During the optimization process with gradient descent the weights of each layer  $i$  are updated as  $w_i = w_{i-1} - \eta \nabla_{w_i} \mathcal{L}(w_1, w_2, \dots, w_n)$ , where  $\nabla_{w_i} \mathcal{L}(w_1, w_2, \dots, w_n)$  is input dependent. As an example, let's consider a two-layer feedforward neural network:

$$\begin{aligned} x &: \text{inputs} \\ l_1 &= W_1 x + b_1 & h &= \text{ReLU}(l_1) \\ h &= \text{ReLU}(l_1) & l_2 &= W_2 h + b_2 \\ \hat{y} &= \text{softmax}(l_2) & J &= \text{CE}(y, \hat{y}) \end{aligned}$$

Analyzing the weights' update below, we can observe that the optimal weights are noisy perturbation of the inputs feature maps and all together they contain information about the training either related to the raw input or the feature map at a given stage.

$$\begin{aligned} \delta_1 &= \frac{\partial J}{\partial l_2} = (y - \hat{y})^T \\ \delta_2 &= \frac{\partial J}{\partial l_1} = \delta_1 W_2 \text{osgn}(h) \\ W_1^{(i+1)} &= W_1^{(i)} - \eta \nabla_{w_1} \mathcal{L}(w_1, w_2, b_1, b_2) \\ &= W_1^{(i)} - \eta \delta_2^T x \\ W_2^{(i+1)} &= W_2^{(i)} - \eta \nabla_{w_2} \mathcal{L}(w_1, w_2, b_1, b_2) \\ &= W_2^{(i)} - \eta \delta_1^T h^T \end{aligned}$$

### A.2 WEIGHTS VECTORIZATION

[] For a neural network with  $L$  layers, the process of vectorizing the weights and biases for both fully connected and convolutional layers is as follows:

- For the  $\ell$ 'th fully connected layer:  $W^{(\ell)} \in \mathbb{R}^{d_{l-1} \times d_l} \rightarrow \text{vec}(W^{(\ell)}) \in \mathbb{R}^{d_{l-1} \cdot d_l}$  and  $b^{(\ell)} \in \mathbb{R}^{d_l}$ , the length of the vectorized weights for this layer, including the bias if it is not null, is given by  $d_{l-1} d_l + d_l$ .
- For the  $\ell$ 'th convolutional layer:  $W^{(\ell)} \in \mathbb{R}^{k_h \cdot k_w \cdot c_{in} \cdot c_{out}}$  and  $b^{(\ell)} \in \mathbb{R}^{c_{out}}$ , the length of the vectorized weights for this layer, including the bias if it is not null, is  $k_h \cdot k_w \cdot c_{in} \cdot c_{out} + c_{out}$ .

We then concatenate all the flattened weight and bias vectors resulting in a vector  $\theta$ :  $\theta = \bigoplus_{l=1}^L (\text{vec}(W^{(l)}) \oplus b^{(l)})$  where  $\text{vec}$  denotes the vectorization operation and  $\oplus$  denotes concatenation. The concatenation operation keeps the ordering of weights in the network.

### A.3 LAYER SELECTION STRATEGY

To manage the large number of parameters in LLM architectures, where not all layers are required to be tuned to improve the performance, we propose focusing on the most important layers. These layers are identified using the Marchenko-Pastur (MP) distribution, which serves as a filter to highlight relevant weights while discarding those resembling random noise. The MP law provides a benchmark for distinguishing structured weights from noise by comparing the empirical eigenvalue spectrum of weight matrices to the MP distribution. D2NKG uses this *spectrum method* (Hartford et al., 2024) to learn the distribution of the most informative weights—those corresponding to eigenvalues that significantly exceed the MP upper bound. By focusing on these critical weights, D2NKG captures meaningful patterns in LLMs, leading to enhanced performance in transfer learning.

The spectrum method, grounded in random matrix theory, applies the Marchenko-Pastur (MP) distribution to different types of layers, treating them as rectangular random matrices. In transformer networks, functionally similar layers are grouped, such as a set for all query layers in multi-head attention. The method begins by computing the covariance matrix of each layer’s weight matrix,  $W \in \mathbb{R}^{m \times n}$ , as  $\Sigma = \frac{W^T W}{n}$ , followed by eigenvalue extraction. Singular value decomposition (SVD),  $W = USV^T$ , is used to efficiently compute these eigenvalues from the diagonal matrix  $S$ , which contains the singular values. The resulting eigenvalues describe the variance captured by each principal component of the squared weight matrix and form what is known as the *empirical spectrum*. To analyze this spectrum, we compare it to the theoretical distribution of eigenvalues predicted by the Marchenko-Pastur (MP) distribution. This distribution  $p(\lambda)$ , in equation 7, characterizes the eigenvalue behavior of random covariance matrices as  $m, n \rightarrow \infty$ , with a fixed aspect ratio  $q = \frac{m}{n}$  and variance  $\sigma^2$ .

$$p(\lambda) = \frac{1}{2\pi\sigma^2q\lambda} \sqrt{(\lambda_+ - \lambda)(\lambda - \lambda_-)}, \quad (7)$$

where  $\lambda \in [\lambda_+, \lambda_-]$ ,  $\lambda_+ = \sigma^2(1 + \sqrt{q})^2$ , and  $\lambda_- = \sigma^2(1 - \sqrt{q})^2$ . From 7, the corresponding bounds for eigen values of  $W$  are  $\sqrt{\lambda}/\sqrt{n} \in [\varepsilon_+, \varepsilon_-]$ ,  $\varepsilon_+ = \frac{1}{\sqrt{n}}\sigma(1 + \sqrt{q})$ , and  $\varepsilon_- = \frac{1}{\sqrt{n}}\sigma(1 - \sqrt{q})$ .

**Interpretation:** The Marchenko-Pastur (MP) distribution provides insight into the underlying structure of data or layer in our case:

- *Eigenvalues within MP bounds:* Likely represent noise, with their corresponding principal components carrying little meaningful information, indicating the layer’s lower importance.
- *Eigenvalues larger than the upper MP bound  $\lambda_+$ :* Capture more variance than noise, suggesting the presence of true signals or patterns in the data.
- *Eigenvalues smaller than the lower MP bound  $\lambda_-$ :* May indicate compression or degeneration in the data structure.

Significant deviations, particularly large eigenvalues, indicate meaningful components that capture more variance than random noise, aiding in the identification of important features or signals. This insight is used to compute the signal-to-noise ratio (SNR), where eigenvalues below the upper bound are considered noise. The SNR is calculated as follows:

$$SNR = \frac{\sum_k |\sigma_k| \geq \varepsilon \sigma_k}{\sum_n |\sigma_n| < \varepsilon \sigma_n}. \quad (8)$$

### A.4 LEARNING THE DISTRIBUTION OF LLM WEIGHTS

Our method for LLM weight generation employs a layer-wise chunking mechanism that facilitates both layer-wise and chunk-wise sampling. Each layer is divided into independent chunks to form the training data, and are then encoded with the VAE. During the diffusion process, an index is assigned to each chunk, and the model is trained using class-conditioned diffusion, where chunk indices serve as class labels. At sampling time, the chunk indices corresponding to each layer are grouped into clusters associated with that layer. These clusters are then used to sample new sets of chunks, which are concatenated to reconstruct the sampled weights for each layer.

After selecting the top 25% of the layers, we applied chunking with a size of 2,097,152 for LLaMA 3.2-1B and 4,194,304 for other models. We then performed sequential refinement using Algorithm

1. Unlike in vision tasks, LLM models are conditioned on chunk indices. Here, we refer to neural network operations such as dense layers and layer normalization as *layers*. The spectrum method provides an ordered set of these layers (q, k, v, o, mlp\_up, mlp\_down, mlp\_gate). For architectures like Llama 3.1-8B and Mistral, we only learn the distribution of the top 8 each of these layers, excluding layer normalization. These layers are further divided into two groups: the top 4 and the second top 4, for which we build separate models to learn their distributions. As for the normalization layers, we learn the distribution across all of them. The maximum generated parameters is  $\approx 872\text{M}$ .

---

**Algorithm 1** Sequential Weight Model Improvement
 

---

```

1: Input: Initial weights  $\Theta_{\text{init}} = \{\tilde{\theta}_1, \dots, \tilde{\theta}_L\}$ , Hypernetwork  $\mathcal{H}_i$  for each layer  $i$ , Validation
   dataset  $\mathcal{D}_{\text{val}}$ ,  $K$  candidates per layer
2: Output: Final weights  $\Theta^* = \{\theta_1^*, \dots, \theta_L^*\}$ 
3: Initialize  $\Theta^* = \Theta_{\text{init}}$ 
4: Compute initial validation accuracy:  $\text{current\_accuracy} = \mathcal{A}(\Theta_{\text{init}}, \mathcal{D}_{\text{val}})$ 
5: for each layer  $i = 1$  to  $L$  do
6:   Generate  $K$  candidates  $\{\theta_i^{(1)}, \dots, \theta_i^{(K)}\}$  using  $\mathcal{H}_i$ 
7:   for each candidate  $k = 1$  to  $K$  do
8:     Replace  $\tilde{\theta}_i$  with  $\theta_i^{(k)}$  in  $\Theta^*$  to form  $\Theta^{(k)}$ 
9:     Compute validation accuracy:  $\mathcal{A}(\Theta^{(k)}, \mathcal{D}_{\text{val}})$ 
10:  end for
11:  Choose  $\theta_i^* = \arg \max_k \mathcal{A}(\Theta^{(k)}, \mathcal{D}_{\text{val}})$ 
12:  if  $\mathcal{A}(\Theta^{(k)}, \mathcal{D}_{\text{val}}) > \text{current\_accuracy}$  then
13:    Update  $\Theta^* = \Theta^{(k)}$ 
14:    Update  $\text{current\_accuracy} = \mathcal{A}(\Theta^*, \mathcal{D}_{\text{val}})$ 
15:  else
16:    Retain  $\tilde{\theta}_i$  in  $\Theta^*$ 
17:  end if
18: end for
19:
20: return  $\Theta^*$ 

```

---

## A.5 MODELZOO AND PRETRAINED DATASETS

**Model zoo** We use the pretrained datasets from Schürholt et al. (2022c) as structured in Schürholt et al. (2022a). This dataset consists of 4 different datasets with 5000 pretrained weights per architectures and datasets. The details of the architecture used to generate the pretrained weights are available in Schürholt et al. (2022c).

**KaggleZoo** This modelzoo is generated using the dataset provided by Jeong et al. (2021). To efficiently generate the pretrained weights, we first compute the features of each image then use a MLP with two layers with input size 512, hidden size 256 and leaky ReLU activation functions. We train the MLP on clip features as it allows us to quickly generate high performing weights. For each datasets we used the last 10 checkpoints which results in 1400 pretrained weights for training.

**ImageNet zoo** To generate the pretrained modelzoo on ImageNet, we sample 1000, 5000, 10000 and 20000 subsets with 10 classes each with 100 images per class in the training set and 50 per class in the test set. For the 1000 and 5000 subsets we used the same MLP architecture as the KaggleZoo. For the 10000 subset, we reduce the hidden dimension to 128 and, for the 20000 subset we use a single linear probing layer. On the other datasets linear probing shows similar generalization performance as the two-layer MLP. We use Adam optimizer with a learning rate of  $1e - 3$  and all models are trained for 30 epochs.

**Zoo for Few-shot learning:** The few-shot learning pretrained zoo is generated by fine-tuning the classifier head for 10 epochs on each of the 50,000 subsets.

**LLMs zoo:** We collected the pretrained LLM model from their original HuggingFace repositories with no further pertaining on specific tasks or datasets.

**Meta-album datasets:** We split the meta-album dataset into a training set (70%) and a test set (30%). Next, we trained the MobileNetV3 OFA subnet with parameters  $d = 2$ ,  $k = 3$ , and  $e = 3$  for 100 epochs. Checkpoints from the last 20 epochs were collected as training data. A detailed breakdown of the dataset can be found in Table 12.

## A.6 DETAILS OF THE PROPOSED MODEL

We build our dataset conditioned weight generation model using latent diffusion (Rombach et al., 2021).

**AutoEncoder:** We use the same VAE modules of latent diffusion and use the same architecture for all experiments except adaptation of the inputs and output dimensions. We insert a linear layer before the first layer of the encoder such that we can reshape its output to a representation for the convolution layers. Similarly, a linear layer is placed at the last layer of the decoder adapting the output to the vectorized weights representations. For the VAE loss function we removed the discriminator in the original latent diffusion VAE loss function.

**Diffusion Model:** We utilize same UNet architecture as in latent diffusion with the same training procedure.

**Dataset Encoding Mechanisms** We investigated three different mechanisms of dataset encoding. Firstly, we use Set Transformer (Lee et al., 2019a) which can be difficult to train when optimized together with the diffusion using the weights encoder from the VAE and the Set Transformer.

In addition to the Set Transformer, we explored a two-layer MLP model as the dataset encoder. The first layer is a dynamic linear layer with a maximum input feature size set to  $n_{\max} \cdot c_{\max}$ , where  $n_{\max}$  is the maximum number of images per class and  $c_{\max}$  is the maximum number of classes among all subsets of the pretrained datasets. The shape of the image features in each dataset obtained with the CLIP image encoder is  $x \in \mathbf{R}^{c \times n \times d}$ , where  $d$  is the feature dimension for each corresponding pretrained weight vector. While the Set Transformer-based encoder uses these inputs directly, the MLP encoder reshapes each input from  $x \in \mathbf{R}^{c \times n \times d}$  to  $x \in \mathbf{R}^{d \times (n \cdot d)}$  and then applies the dynamic linear layer. If a dataset has more classes or samples than  $c_{\max}$  and  $n_{\max}$  respectively, we only consider the first  $c_{\max}$  classes and  $n_{\max}$  samples per class. If the dataset has fewer classes or samples, we adjust the dynamic linear layer dimensions accordingly. The output of the dynamic linear layer is  $z \in \mathbf{R}^{d \times h}$ , where  $h$  is an arbitrarily chosen number greater than zero. We then reshape  $z$  from  $\mathbf{R}^{d \times h}$  to  $\mathbf{R}^{1 \times (h \cdot d)}$  (with  $h \cdot d$  fixed) and apply the final linear layer to obtain the desired output. This model can be jointly optimized with the diffusion model while achieving good performance.

**Dataset Encoding with Set Transformer** We use the Set Transformer for dataset encoding, pretrained as described in Lee et al. (2021). The approach involves using the frozen Set Transformer and adding a single linear layer to adapt its output to our specific problem, utilizing it as the dataset encoder. This method reduces the computational cost of training the Set Transformer and enables joint optimization of the dataset encoder and the diffusion model. The results of these data set encoding schemes are presented in Table 21 for the Hyperzoo dataset.

Table 8: Models setting,  $n$  and  $c$  in the dataset configuration represent respectively the number of samples per class  $n=5$  for training and  $c$  the total number of classes per dataset. The VAE and the diffusion models share similar configuration and architectures as (Rombach et al., 2021)

Parameters	Values
Epochs	[50, 2000]
VAE	
Optimizer	Adam
Learning Rate	1e-3
Latent Dimiension	1024
KL-Divergence Weight	1e-6
Dataset Encoder	
Architecture	Set Transformer
Input Dimension	$c \times n \times 512(\min)$
Output Dimension	1024 (min)
Depth of Set Transformer	2
Diffusion	
Optimizer	AdamW
Learning Rate	1e-4
Scheduler	Linear
Time step	1024
Network	Unet
UNet Input Size	$(c \times 32 \times 32)$

**Algorithm 2** Datasets Encoder Training

1080  
1081  
1082  
1083  
1084  
1085  
1086  
1087  
1088  
1089  
1090  
1091  
1092  
1093  
1094

```

Input: pretrained weights  $x$ , image features  $y$ , batch_num  $m$ 
Instantiate  $\mathcal{T} = \text{Set Transformer}$ , Load pretrained Encoder ( $\mathcal{E}$ ).
repeat
  Initialize  $loss = 0.0$ 
  for  $i = 1$  to  $m - 1$  do
     $x_i \sim x, \mathcal{D}_i \sim \mathcal{D}$ 
     $z_i = \text{Encoder}_{\text{VAE}}(x_i)$ 
     $z_{\mathcal{D}_i} = \mathcal{T}(\mathcal{D}_i)$ 
     $loss = loss + \mathcal{L}_{\text{CLIP}}(z_i, z_{\mathcal{D}_i})$  (Equation ??)
  end for
  Update weights of  $\mathcal{T}$ 
until convergence
    
```

1095  
1096  
1097  
1098  
1099  
1100  
1101  
1102  
1103  
1104

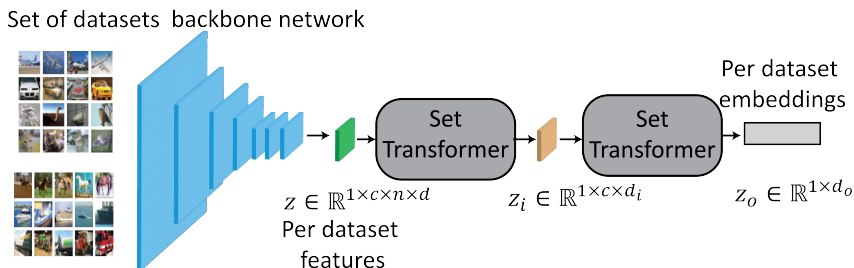


Figure 5: Overview structure of the set-transformer-based dataset encoder. For each pretrained dataset we use  $n = 5$  images per class and the embedding dimension  $d_0 = 1024$ .

1105  
1106  
1107  
1108  
1109  
1110

**B TRAINING DETAILS**

In this section, we describe the training steps used to train our method.

1111  
1112  
1113  
1114  
1115  
1116  
1117  
1118  
1119  
1120  
1121  
1122  
1123  
1124  
1125  
1126

- **Pretrained Zoo Generation:** For classifier head adaptation, we first compute the features for all datasets. Then, we train the classifier head to generate the pretrained zoo.
- **VAE Training:** We train the VAE to encode the pretrained weights following Equation 1. Additionally, a pretrained performance predictor can be used to predict the performance of the reconstructed weights and guide the VAE training as described in Equation 9.
- **Dataset Alignment:** If using dataset alignment, we pretrain the Set Transformer to align the pretrained weights’ latent representations. This is done using the frozen encoder of the VAE and the dataset embeddings. The inputs to the Set Transformer are image features, with five image features per class.
- **Diffusion Process Training:** We train the diffusion model while keeping the Set Transformer and the VAE models frozen. If an MLP is used for dataset encoding, we jointly optimize the diffusion process with the MLP dataset encoder.

1127  
1128  
1129  
1130  
1131  
1132  
1133

Although the dataset encoder can be optimized together with diffusion model, we train them separately to speed up the training process and reduce memory requirements. The VAE and the dataset encoder are trained using the Adam optimizer with a learning rate of  $1e - 4$ . The diffusion model in each experiment is trained with a linear scheduler, a base learning rate of  $1e-4$ , and the AdamW optimizer (Rombach et al., 2021). During the training process of the diffusion model, the output of the dataset encoder is concatenated with the latent representation of the input weights, forming the input to the UNet model. Additionally, we investigate joint training of the diffusion process in the ablation study and Appendix C.5 and A.6. Further details can be found in Table 8.

**Algorithm 3** Predictor-Guided VAE

---

**Input:** Pretrained weights  $x$ , accuracy  $y$ , batch\_num  $m$   
 Instantiate  $f =$  Set Transformer, and load pretrained predictor  $g$ .  
**repeat**  
   Initialize  $loss = 0.0$   
   **for**  $i = 1$  **to**  $m - 1$  **do**  
      $\bar{x} = f_{\theta}(x)$ ,  $\bar{y} = g(\bar{x})$   $\hat{y} = g(x)$   
      $L_{\theta} \frac{x - \bar{x}}{\sigma^2} + \log \sigma^2 + \|\hat{y} - \bar{y}\|^2$   
   **end for**  
   Update weights of  $f$   
**until** Convergence

---

## B.1 PREDICTOR TRAINING

To improve the reconstruction and sampling efficiency, we trained an accuracy predictor  $g$  from pretrained weights  $w$  then use the frozen predictor during the training of the VAE as a regularizer as shown below:

$$\min_{\theta, \sigma} \frac{w - f_{\theta}(w)}{\sigma^2} + \log \sigma^2 + \|g(w) - g(f_{\theta}(w))\|^2, \quad (9)$$

where  $g(w)$  is the embedding of the original input and  $g(f_{\theta}(w))$  is the predictor embedding of the reconstructed weights. The predictor can be either dataset-conditioned or unconditioned. In general we found that dataset-conditioned predictor works only well for large number of samples per dataset. After the AutoEncoder is trained, we train the dataset-conditioned module which requires a dataset encoder.

## C ABLATION STUDY

## C.1 CAN THE PROPOSED METHOD HANDLE MULTIPLE ARCHITECTURES?

This section provides a simple way to handle the case where the pretrained zoo contains multiple architectures per task or dataset. Since the number of architecture and dataset are predefined, it is possible to build a set of unique index for each combination of dataset-architecture pairs. An alternative will be to encode the graph representation of the architectures then used that as conditioning. In this ablation study we use the simple class indexing approach to demonstrate the versatility of our method. We use CIFAR10 and CIFAR100 as the dataset and as target architectures we utilize a ResNet44 trained on CIFAR-100 with 667,188 parameters and a ResNet44 trained on CIFAR-10 with 661,338 parameters and finally, a MobileNetV2 trained on CIFAR-10 with 700,490 parameters. All models were zero-padded to 700,490 parameters, combined into a unified dataset, and trained without chunking. The results in Table 9 demonstrate that the proposed method is capable of simultaneously learning the distributions of diverse architectures trained on diverse datasets.

Model	ResNet44 (CIFAR-10)	ResNet44 (CIFAR-100)	MobileNetV2 (CIFAR-10)
Pretrained	94.01	71.63	92.88
D2NWG	94.10 $\pm$ 0.09	71.64 $\pm$ 0.02	93.11 $\pm$ 0.20

Table 9: Performance evaluation on mixed architectures.

## C.2 TRANSFERABILITY

As demonstrated in Table ??, our approach achieves performance comparable to existing methods while relying on a **single generative model** instead of 38 task-specific pretrained models. Notably, the pretrained model architecture and parameter counts used in this study are publicly available on a non-affiliated GitHub repository: <https://github.com/chenyaofu/pytorch-cifar-models>.

1188 EVALUATING SAMPLING FOR TRANSFER LEARNING  
 1189

1190 We compared sampling from a distribution of diverse pretrained models against traditional single-  
 1191 model transfer learning, using **ResNet-56** and our generative model trained on weights from 19  
 1192 diverse architectures pretrained on CIFAR-10 and CIFAR-100. We tested three experimental setups:

- 1193 1. **Direct evaluation** of the pretrained models.
- 1194
- 1195 2. **Sampling conditioned on training sets** (e.g., STL-10, CIFAR-10).
- 1196

1197 **Results** show that our approach consistently outperforms single-model transfer learning. Notably,  
 1198 there is no significant difference between training- and test-conditioned sampling when drawn from  
 1199 the same distribution, demonstrating the robustness of our method. This highlights the practicality of  
 1200 leveraging diverse pretrained model distributions for improved generalization.

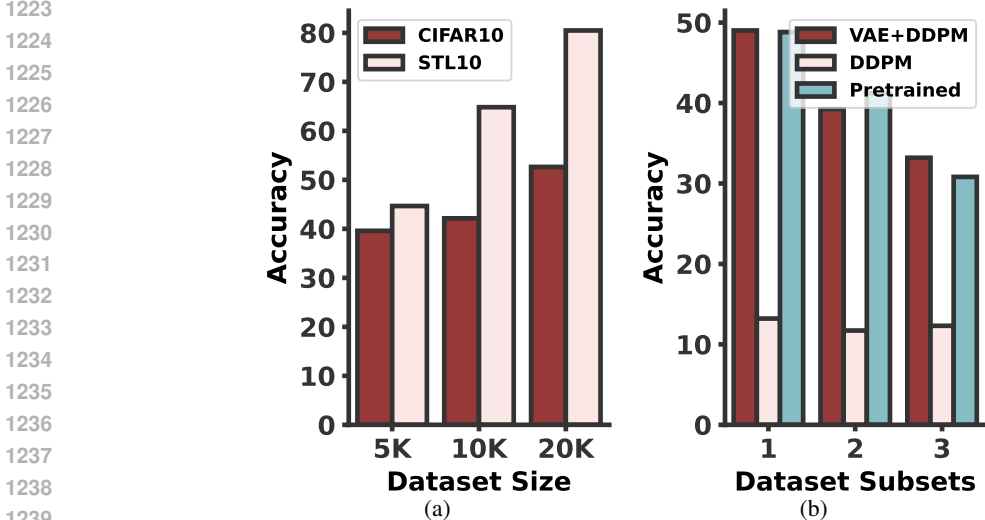
1201  
 1202 Table 10: Performance on CIFAR10.1 and STL10 of D2N WG trained on diverse architectures

Model	CIFAR10.1	STL10
Pret-cifar10	75.20	32.37
Pret-cifar100	0.25	0.12
Ours	83.10 ± 0.06	35.41 ± 0.13
Ours(test)	83.04 ± 0.06	35.47 ± 0.12

1210  
 1211 C.3 EFFECT OF MODELZOO SIZE GENERALIZATION  
 1212

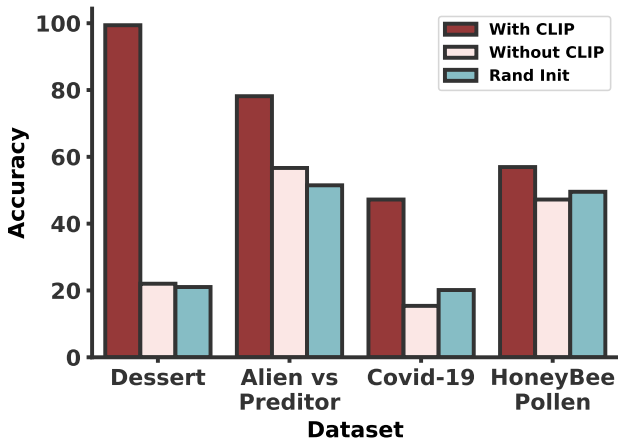
1213 Here we investigate the impact of increasing the number of pretrained datasets on performance  
 1214 with experiments that use model zoos of sizes 5000, 10,000, and 20,000, derived from ImageNet  
 1215 subsets. Unseen target datasets CIFAR-10 and STL-10 are used. Sampling 50 weights, the average  
 1216 performance of the top 5 performing weights is shown in Figure 6a.

1217 **Results:** On CIFAR-10 and STL-10, we obtain accuracies of  $39.60 \pm 1.31\%$  and  $44.66 \pm 0.55\%$   
 1218 for 5000 subsets,  $42.15 \pm 2.12$  and  $64.83 \pm 2.83\%$  for 10000 subsets, and  $52.64 \pm 3.12\%$  and  
 1219  $80.49 \pm 1.77\%$  for 20000 subsets. The maximum accuracies with random initialization are 12.11%  
 1220 and 17.12% on CIFAR-10 and STL-10 without fine-tuning. This experiment demonstrated that  
 1221 increasing the number of datasets enhances the generalizability of the proposed method.



1240 Figure 6: (a) Effect of the number of pretrained datasets on sampling weights performance on unseen datasets.  
 1241 (b) Performance comparison on in-distribution sampling of methods with VAE+DDPM vs DDPM

1242  
1243  
1244  
1245  
1246  
1247  
1248  
1249  
1250  
1251  
1252  
1253  
1254  
1255  
1256



1257 Figure 7: Performance comparison at initialization of method with jointly trained set-transformer (Without  
1258 CLIP) and method clip-based dataset encoder.

#### 1259 C.4 SAMPLING WITHOUT LATENT REPRESENTATION

1260 This section explores a model variant that directly learns the diffusion model on weights, bypassing  
1261 the AutoEncoder stage, and compares it to the standard approach. Both variants are trained on  
1262 1000 subsets of ImageNet, and evaluated in in-distribution sampling setting on three randomly  
1263 selected subsets from the 1000 subsets. The results, presented in Figure 6b, indicate that learning  
1264 the distribution of pretrained weights in the latent space is notably successful in generating high-  
1265 performing weights. The failure of the DDPM process on raw pretrained weights may stem from  
1266 their higher model capacity requirement.

#### 1267 C.5 CLIP-BASED DATASET ENCODING

1268 In this section, the comparison between the CLIP-based dataset encoding scheme trained at an  
1269 intermediate stage and the Set Transformer encoder jointly trained with the diffusion process is  
1270 explored. Experiments are conducted on 140 Kaggle datasets and their respective model zoos. The  
1271 results depicted in Figure 7 indicate that both methods achieve similar results for small numbers of  
1272 datasets during the in-distribution sampling. However, as the number of datasets increases, the Set  
1273 Transformer jointly trained with the diffusion approach faces challenges in convergence and requires  
1274 more computational resources, as demonstrated in Figure 7.

#### 1275 C.6 UNCONDITIONAL SAMPLING

1276 We conduct the experiment using ResNet18 pretrained on CIFA-100 and CIFAR-10. For all datasets,  
1277 the weight vector length is 2048 and we compare with pdiff (Wang et al., 2024). While pdiff requires  
1278 a separate model for each dataset, our method combines the pretrained weights into a single dataset  
1279 and conditionally learns their distribution. The sample size for each dataset in our method is 200,  
1280 with a combined total of 400 parameters. The results are provided in Table 11 for 100 sampled  
1281 weights. Two separate models for are trained for pdiff, CIFA10-pdiff and CIFAR100-pdiff while  
1282 our method consists of a single model trained once for both datasets. It can be seen that our method  
1283 outperformance the baseline (Wang et al., 2024) in Table 11.

1284 Table 11: Unconditional Sampling Evaluation against Wang et al. (2024) on ResNet18.

Dataset	CIFAR-10				CIFAR-100				Runtime
	Avg	Median	Max	#Epochs for VAE,DDPM	Avg	Median	Max	#Epochs for VAE,DDPM	
pdiff	94.46	94.46	<b>94.52</b>	8999,47999	76.1028	76.13	76.21	32999,38999	$\approx 3h$
D2NKG	94.46	<b>94.47</b>	94.50	100,200	<b>76.1796</b>	<b>76.18</b>	76.24	100,200	$\approx 1h30$

1288  
1289  
1290  
1291  
1292  
1293  
1294  
1295



### 1296 C.7 COUPLING WITH AN ACCURACY PREDICTOR

1297  
1298 This section reports the extended results of Table 19 in which we compared our method in-distribution  
1299 and out-of distribution with and without accuracy predictor.

1300 **Results.:** The full results of Table 19 are reported in Table 20. Using an accuracy predictor enable  
1301 easily selecting highly performing when sampling in-distribution. However, in our case the accuracy  
1302 predictor struggles to generalize well for unseen dataset as shown in Table 20  
1303

### 1304 C.8 SAMPLED WEIGHTS ANALYSIS

1305  
1306 In this section, we analyze the characteristics of the sampled weights and compare them to the  
1307 pre-trained ones based on experiments with the model zoo and a model pre-trained on a subset of  
1308 ImageNet. The proposed method samples weights with a large variance, as shown in Figure 10,  
1309 providing a broad range of initialization choices, from weights with low initial performance to those  
1310 with higher initial performance.  
1311

1312  
1313 Table 12: Details description of meta-album datasets

1314 Domain	1315 Original Dataset	1316 # Classes
1317 Large Animals	1318 Animals with Attributes, Dogs, 1319 Birds	1320 50, 120, 315
1321 Small Animals	1322 Insects, Insects 2, Plankton	1323 117, 102, 102
1324 Plants	1325 Fungi, PlantNet, Flowers	1326 25, 25, 102
1327 Plant Diseases	1328 PlantDoc, Medicinal Leaf, 1329 Plant Village	1330 27, 26, 38
1331 Microscopy	1332 Subcel. Human Protein, Pan- 1333 Nuke, Bacteria	1334 21, 19, 33
1335 Remote Sensing	1336 RSD, RSICB, RESISC	1337 43, 45, 45
1338 Vehicles	1339 Boats, Airplanes, Cars	1340 26, 21, 196
1341 Manufacturing	1342 Textures ALOT, Textures 1343 DTD, Textures	1344 250, 47, 64
1345 Human Actions	1346 MPII Human Pose, Stanford 1347 40 Actions, 73 Sports	1348 29, 40, 73
1349 OCR	1350 Omniprint-MD-6, Omniprint- 1351 MD-5-bis, Omniprint-MD- 1352 mix	1353 703, 706, 706

### 1335 C.9 EVALUTAION ON LARGE DATASETS

1336  
1337 We investigate how our method perform for combined large and small dataset as well for mixed  
1338 architectures. For this experiment we collect the pretrained weights from PyTorch hub with one  
1339 checkpoints per datasets(CIFAR-10, CIFAR-100, and ImageNet-1k). After conditionally learning  
1340 the combined weights distribution, we sampled 10 weights for each datasets and report the average  
1341 accuracy of the top-3 datasets in Table 15. As shown in Table 15, D2NKG consistently produced  
1342 high performing weights for each dataset from a single pretrained checkpoint.  
1343

### 1344 C.10 GENERATING THE FULL WEIGHTS FOR RESNET18

1345  
1346 We investigate how our method performs when used to generate the full parameters for a ResNet18  
1347 model pretrained on MNIST, CIFAR-10, and CIFAR-100. In total, we use 100 pretrained weights per  
1348 dataset and conditionally learn their distribution. The modelzoo generation follows the same setting  
1349 as Wang et al. (2024). Table 16 demonstrates the effectiveness of our method for generating the entire  
weights of a network.

Table 13: Comparison between Base Model and Improved Model Responses

Instruction	Base Model Response	Improved Model Response
<p>Prompt: {"role": "system", "content": "You are an AI chatbot"}, {"role": "user", "content": "Explain what AI is and its importance"}.</p>	<p><b>What is AI?</b> Artificial Intelligence (AI) refers to the development of computer systems that can perform tasks that would typically require human intelligence, such as:</p> <ol style="list-style-type: none"> <li><b>Learning:</b> AI systems can learn from data, experiences, and environments to improve their performance.</li> <li><b>Reasoning:</b> AI systems can reason and make decisions based on the data they have learned.</li> <li><b>Problem-solving:</b> AI systems can solve complex problems and adapt to new situations.</li> <li><b>Perception:</b> AI systems can perceive and understand the world around them through sensors, cameras, and other devices.</li> </ol> <p>AI systems use various techniques, such as machine learning, deep learning, natural language processing, and computer vision, to achieve these capabilities.</p> <p><b>Types of AI:</b></p> <ol style="list-style-type: none"> <li><b>Narrow or Weak AI:</b> Designed to perform a specific task, such as facial recognition or language translation.</li> <li><b>General or Strong AI:</b> Designed to perform any intellectual task that a human can, such as reasoning, problem-solving, and learning.</li> <li><b>Superintelligence:</b> Significantly more intelligent than the best human minds, potentially leading to exponential growth in technological advancements.</li> </ol> <p><b>Importance of AI:</b></p> <ol style="list-style-type: none"> <li><b>Automation:</b> AI can automate repetitive and mundane tasks, freeing up human resources for more strategic work.</li> </ol>	<p><b>What is Artificial Intelligence (AI)?</b> Artificial Intelligence (AI) is a branch of computer science that focuses on creating intelligent machines that can think, learn, and behave like humans. AI involves the development of algorithms, statistical models, and computer programs that enable machines to perform tasks that typically require human intelligence, such as:</p> <ol style="list-style-type: none"> <li><b>Reasoning and problem-solving:</b> AI systems can analyze data, identify patterns, and make decisions based on that data.</li> <li><b>Learning:</b> AI systems can learn from experience, adapt to new situations, and improve their performance over time.</li> <li><b>Perception:</b> AI systems can interpret and understand data from sensors, such as images, speech, and text.</li> <li><b>Natural Language Processing (NLP):</b> AI systems can understand and generate human language, enabling them to communicate with humans.</li> </ol> <p><b>Importance of AI</b> AI has become increasingly important in various aspects of our lives, including:</p> <ol style="list-style-type: none"> <li><b>Automation:</b> AI can automate repetitive and mundane tasks, freeing up human time for more creative and strategic work.</li> <li><b>Improving decision-making:</b> AI can analyze large datasets, identify patterns, and provide insights that inform business decisions.</li> <li><b>Enhancing customer experience:</b> AI-powered chatbots and virtual assistants can provide 24/7 support and personalized services.</li> </ol>
<p>prompt: {"role": "system", "content": "You work at a coffee shop"}, {"role": "user", "content": "what title do you give to someone who serves the coffee to customers"}.</p>	<p>At our coffee shop, we call the person who serves the coffee to customers a 'Barista'. However, some of our team members are also referred to as 'Cafe Attendants' or 'Coffee Servers', depending on their specific role and responsibilities. But generally, the title 'Barista' is the most commonly used and well-known term in the industry.</p>	<p>In a coffee shop, the person who serves the coffee to customers is typically referred to as a: Barista: This is the most common title, and it refers to a skilled person who prepares and serves coffee drinks, as well as other beverages and food items. Coffee Server: This title is also used to describe someone who serves coffee and other beverages to customers. Coffee Barista or Coffee Specialist: These titles are often used in specialty coffee shops or high-end establishments to emphasize the barista's expertise and knowledge of coffee. In our coffee shop, I'm a barista, and I'm happy to serve you your favorite coffee drink.</p>

### C.11 GENERATING WEIGHTS FOR MOBILENETV3

So far, our focus has been on model zoos populated by relatively simple classifier heads. In this section, we evaluate our method using MobileNetV3, a subnetwork sampled from OFA (Cai et al., 2020), consisting of 2.8 million parameters fine-tuned on CIFAR-10, STL-10, SVHN and MNIST for 15 epochs. We collect the last 10 checkpoints per dataset and utilize our method to learn the distribution of pretrained weights. Furthermore, we combine the pretrained weights of MNIST and CIFAR-10, learn their distribution, and then evaluate our method on SVHN and STL-10. Subsequently, we reverse this process by combining the pretrained weights of SVHN and STL-10, and evaluate our method on MNIST and CIFAR-10.

Table 14: Glue benchmark tasks descriptor used in the experiment on glue datasets.

Task Name	Description
<b>SSTB</b>	Predict the similarity score between two sentences. Rate their similarity on a scale from 0 to 5, where 0 indicates no meaning overlap, 1 indicates very little overlap, and 5 indicates complete overlap in meaning.
<b>MRCP</b>	Determine the semantic equivalence of two given sentences (Sentence 1 and Sentence 2). If the sentences are semantically equivalent, return 1. If they are not, return 0.
<b>SST2</b>	Determine the sentiment of a given sentence. Respond with 0 if the sentiment is negative and 1 if the sentiment is positive.
<b>COLA</b>	Evaluate whether the given sentence is both syntactically and semantically correct. If it is, respond with "1"; otherwise, respond with "0".
<b>QNLI</b>	Evaluate whether the given response properly answers the provided question. If the response answers the question correctly, return 0; otherwise, return 1.
<b>RTE</b>	Determine if a given hypothesis is true (entailment), false (contradiction), or undetermined (neutral) based on a provided premise.

Table 15: Evaluation on Large Datasets

Datasets	CIFAR10 (ShuffleNet)		CIFAR100 (ShuffleNet)		ImageNet-1k (SqueezeNet)	
	Top1	Top5	ToP1	Top5	Top1	Top5
Pretrained	92.98	99.73	72.39	91.46	58.178	80.624
Ours(sampling)	<b>93.14 ± 0.25</b>	<b>99.76 ± 0.22</b>	<b>72.60 ± 0.15</b>	<b>91.29 ± 0.13</b>	<b>58.257 ± 1.022</b>	<b>81.01 ± 1.251</b>

As shown in Table 23 our method enhances the performance of the pretrained model. Furthermore, we note that learning the full model weights does not compromise performance. Although learning the distribution of the classifier head is computationally efficient, it can result in lower performance.

## C.12 GENERATING WEIGHTS FOR VISION TRANSFORMERS

Our method shows the ability to learn the distribution of all parameters within a vision transformer, including convolutional and linear layers. We present in-distribution evaluation results in plot Figure 9, highlighting the learning of combined weight distributions conditioned on individual datasets. The model zoo for ViTs is collected based on models proposed by [Gani et al. \(2022\)](#).

## D APPLICATION TO LARGE LANGUAGE MODEL (LLM) OUTPUT LAYER GENERATION

**Phi-3-MINI-4K-Instruct:** We conduct experiments on the Microsoft Phi-3-MINI-4K-Instruct model to demonstrate the scalability of our method for generating output layers in large language models (LLMs). The model’s 98.5 million-parameter output layer was split into 96 chunks, each of size 1,026,048, and used as training data for a Variational Autoencoder (VAE) with an embedding size of 1,024. Lacking access to original training data, we used a class-conditional diffusion process, with chunk embeddings as conditioning data. Post-training, conditioned chunks were sampled and

Table 16: **Zero-Shot Transfer Learning** This Table represent results of zero-shot evaluation against the pretrained model on Resnet18 full model architecture.

Model	MNIST	CIFAR-10	CIFAR-100
Pretrained	99.61	94.56	75.86
D2NKG(ours)	99.62 ± 0.07	94.57 ± 0.00	75.83 ± 0.02

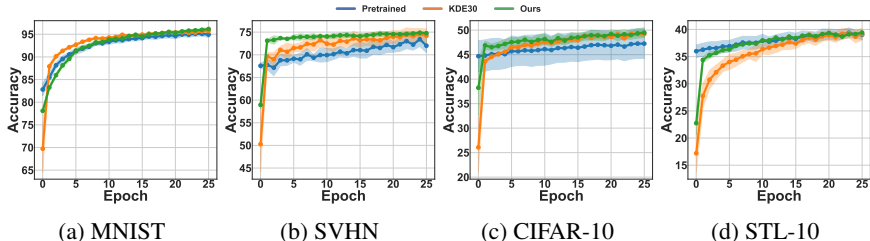


Figure 8: **Convergence Plots on Finetuning Generated Weights:** Weights generated by the competing methods are finetuned for 25 epochs on the training set. We utilize the modelzoos of Schürholt et al. (2022c).

concatenated to reconstruct the original output vector. We evaluate our method using the Open-LLM LeaderBoard-1. As shown in Table 17, our approach effectively scales to the LLMs head generation demonstrating adaptability across diverse domains with minimal adjustments to conditioning data.

Table 17: Generating weights for the Microsoft Phi-3 language model output head.

Methods	ARC Challenge (25-shots)	ARC Easy (25-shots)	HellaSwag (10-shots)	Winogrande (5-shots)
Pretrained	87.16 ± 0.00	63.23 ± 0.01	73.65 ± 0.01	76.64 ± 0.01
D2NKG	87.36 ± 0.01	63.74 ± 0.01	73.65 ± 0.00	76.72 ± 0.01

**GPT2:** In this experiment, we show that our method can learn the distribution of any layer in an LLM by modeling the full distribution of GPT-2 small (164M parameters). We use a chunk size of 1,523,712 and, unlike Llama architectures, concatenated all vectorized layer weights before chunking them uniformly. Table 18 highlights the method’s effectiveness on the Open LM-Leaderboard benchmark. While it did not outperform the base model overall, it significantly improved performance on certain tasks and maintained average accuracy comparable to the pretrained model.

### D.1 FAST CONVERGENCE PERFORMANCE EVALUATION

In this section we report supplementary results for experiment on tiny model zoo dataset. The pretrained weights used here are from epochs 21 to 25 for each dataset where 70% of the resulting modelzoo is used for training and 15% for validation and testing respectively. The number of pretrained weights in the modelzoos are 3500 for MNIST, CIFAR-10, and STL-10, and 2864 for SVHN. The flattened network weights’ length is 2864 for CIFAR-10 and STL-10 and, 2464 for MNIST and SVHN. We pad all the weights with zero to 2864.

### D.2 SAMPLING WEIGHTS FOR UNSEEN DATASETS

**Task:** We evaluate the transferability of the models on unseen datasets. We create disjoint modelzoos by combining MNIST and CIFAR-10 into a single modelzoo and combining the SVHN and STL-10 modelzoos. When we train on the MNIST plus CIFAR-10 modelzoos, we test on the SVHN and STL-10 modelzoos and vice-versa.

**Results:** As shown in Table 19, D2NKG is able to sample weights with higher accuracy on unseen datasets as well as for in distribution. Through these experiments our method does not only outperform the baseline it also demonstrates promising results for dataset-conditioned sampling for unseen datasets.

Table 18: Performance evaluation on unseen open llms leaderboard v2 benchmark base on full gpt2-164M small. These results are produced by Huggingface after submission to open LLM leaderboards.  $\uparrow$  indicate performance improvement while  $\downarrow$  indicate a performance decrease

Method	ifeval (0)	Bbh (3)	Gpqa (0)	MATH-hard (4)	Musr (0)	MMLU-Pro (5)	Avg	Base Model	Fine-tuned
openai-community-gpt2	17.8	2.83	<b>1.12</b>	0.3	<b>13.91</b>	1.84	6.3	na	Yes
D2NWG	<b>19.16</b> ( $\uparrow$ 1.36)	<b>2.85</b> ( $\uparrow$ 0.02)	1.01( $\downarrow$ 0.11)	<b>0.38</b> ( $\uparrow$ 0.08)	12.68( $\downarrow$ 1.23)	<b>1.68</b> ( $\downarrow$ 0.16)	6.29( $\downarrow$ 0.01)	openai-community-gpt2	No

Table 19: **No Fine-tuning Initialization on Unseen Datasets** We transfer from one dataset, or combinations of datasets, to unseen datasets at test time.

Source	Target	Accuracy	Methods
MNIST	SVHN	13.25	$S_{KDE30}$
SVHN	MNIST	29.30	
CIFAR-10	STL-10	15.20	
STL-10	CIFAR-10	15.40	
Sampling from Combined Weights Distribution			
MNIST+CIFAR-10	SVHN	18.80	Ours
MNIST+CIFAR-10	STL-10	16.21	
SVHN + STL-10	MNIST	36.64	
SVHN + STL-10	CIFAR-10	18.00	

## E MISCELLANEA

In Table 24 we present the parameter count for the model used to learn the distribution of the 25% of llama-3.2-1B transformer blocks. In Table 25 we showcase the set of experiments and the corresponding number of parameters generated by D2NWG. Although D2NWG is capable of generating up to 1 billion parameters, all our experiments were limited to a maximum of 872 million, achieved using the Llama 3.1-8B model with 4 transformer layers, excluding layer normalization, for which we constructed a separate model. This parameter count makes D2NWG the only method, to the best of our knowledge, capable of generating nearly a billion parameters, significantly enabling large architecture weights generation including GPT-2 and most existing image classification models in terms of parameter scale. For non-LLM models, we utilize joint distribution learning, enabling task or dataset-conditioned sampling. For example, CIFAR-10 and ImageNet are considered two separate datasets, while SST-2 and CoLA in the GLUE benchmark are treated as two distinct tasks, regardless of differences in the number of classes or subtasks within each dataset or task. Table 25 highlights that the proposed method supports text and image conditioning, as well as layer- or chunk-wise conditional sampling. D2NWG is one of the first weight generation methods to produce over 800 million parameters in a single instance without tiling. Additionally, it is among the first to effectively explore weight generation across various domains, learning the distribution of combined models pretrained on diverse tasks or datasets.

Model	MNIST	SVHN	CIFAR-10	STL-10
Pretrained	99.42 $\pm$ 0.05	94.62 $\pm$ 0.18	93.51 $\pm$ 0.16	94.01 $\pm$ 0.10
Linear_prob	96.88 $\pm$ 0.45	57.23 $\pm$ 0.28	82.85 $\pm$ 0.25	95.63 $\pm$ 1.23
D2NWG(full)	<b>99.55 <math>\pm</math> 0.02</b>	<b>95.13 <math>\pm</math> 0.10</b>	<b>94.23 <math>\pm</math> 0.27</b>	94.02 $\pm$ 0.10
D2NWG(rob)	97.56 $\pm$ 0.26	57.41 $\pm$ 0.17	83.64 $\pm$ 0.47	<b>95.74 <math>\pm</math> 0.74</b>
Cross datasets transfer learning				
OFA (Pretrained)Cai et al. (2020)	13.34	8.90	13.34	8.90
D2NWG(full)	<b>66.82 <math>\pm</math> 0.65</b>	<b>35.20 <math>\pm</math> 0.65</b>	<b>36.70 <math>\pm</math> 0.18</b>	<b>51.50 <math>\pm</math> 0.37</b>
D2NWG(prob)	42.86 $\pm$ 0.62	20.974 $\pm$ 0.78	26.56 $\pm$ 1.22	47.33 $\pm$ 0.32

Table 23: MobileNet Weight Generation.

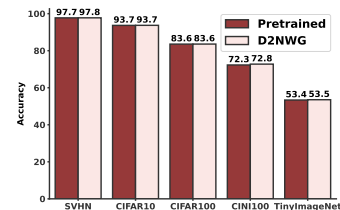


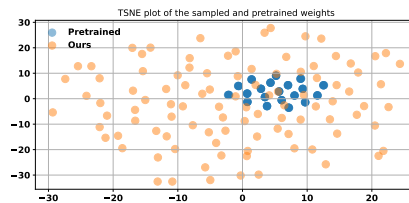
Figure 9: Experiment with ViT

Table 20: Performance evaluation at initialization without fine-tuning. For the baseline we use weights of SVHN for MNIST and vice versa similarly for CIFAR-10 and STL-10

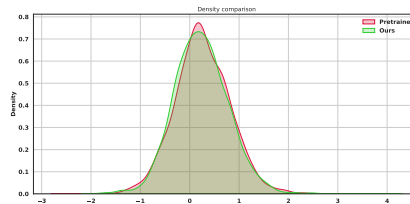
Datasets	MNIST	SVHN	CIFAR10	STL10
Random	10.23±0.56	12.21±3.76	9.98±1.47	9.56±1.02
Pretrained models	82.82± 1.38	<b>67.57± 0.59</b>	<b>44.68± 3.15</b>	<b>35.99± 1.15</b>
$S_{kde30}$ Schürholt et al. (2022a)	69.73± 5.12	50.25± 6.12	26.06± 3.01	17.20± 3.43
seen (D2NWG)	83.92±1.92	61.81 ± 3.13	43.08±0.55	31.45±0.35
seen(D2NWG)(with Pred)	84.85±0.83	66.03 ± 1.36	43.89±0.15	34.29±0.13
$S_{kde30}$ Schürholt et al. (2022a)(cross)	29.30± 3.46	13.25± 1.12	15.40± 0.51	15.20±1.24
not seen(D2NWG)	36.64±4.69	18.80±0.58	18.00±0.22	16.21±0.52
not seen(D2NWG)(with Pred)	30.15±5.09	15.76±1.43	17.10±1.12	15.37±0.52

Table 21: In-distribution performance comparison of different image dataset encoding schemes on model zoo dataset

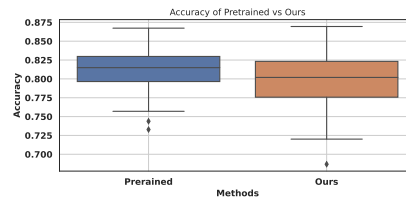
Datasets	MNIST	SVHN	CIFAR10	STL10
Pretrained models	82.82± 1.38	<b>67.57± 0.59</b>	<b>44.68± 3.15</b>	<b>35.99± 1.15</b>
$S_{kde30}$ Schürholt et al. (2022a)	69.73± 5.12	50.25± 6.12	26.06± 3.01	17.20± 3.43
MLP_Encoder	67.04±17.73	35.65 ± 13.03	17.41±3.02	20.36±7.38
Set_transf(pret)	78.21±1.76	60.90 ± 1.08	28.68±1.84	34.75±00.38
seen (D2NWG)	83.92±1.92	61.81 ± 3.13	43.08±0.55	31.45±0.35
seen(D2NWG)(with Pred)	84.85±0.83	66.03 ± 1.36	43.89±0.15	34.29±0.13



(a) TSNE



(b) Density



(c) Accuracy

Figure 10: Analysis of relationship between the pretrained weights and the sampled weights for MNIST dataset

Table 22: Performance of the datasets conditional sampling on 10 unseen real-world datasets. We report the averaged accuracy on ten unseen test datasets over 3 different runs fine-tuned for 50 epochs. pret(imnet): pretrained on imagenet1k

Datasets	No-fine-tuning			50 epochs Fine-Tuning			# of classes
	Random init.	pret(imnet)	D2NKG(ours)	Random init.	pret(imnet)	D2NKG(ours)	
Gemstones	1.13 ± 0.52	0.62 ± 0.00	<b>1.86 ± 0.25</b>	70.59±0.91	67.49±0.43	<b>76.06 ± 0.88</b>	87
Dog Breeds	0.55 ± 0.22	0.69 ± 0.00	<b>1.87 ± 0.39</b>	80.78±0.28	78.13±0.49	<b>80.88 ± 0.88</b>	133
Dessert	21.03 ± 2.44	12.50 ± 0.00	<b>99.40 ± 0.02</b>	95.83±0.34	94.64±0.00	<b>99.40 ± 0.02</b>	5
Colorectal Histology	11.77 ± 2.88	11.00 ± 0.00	<b>18.12 ± 0.25</b>	90.34 ± 0.33	89.75±0.19	<b>93.65 ± 0.10</b>	8
Drawing	10.86 ± 1.22	11.00 ± 0.00	<b>11.87 ± 0.93</b>	<b>90.20 ± 0.16</b>	90.00±0.16	89.00 ± 0.16	10
Alien vs Predator	51.48 ± 2.09	28.88 ± 0.00	<b>78.15 ± 0.52</b>	98.52±0.52	<b>98.89 ± 1.42</b>	97.77 ± 0.00	2
COVID-19	20.13 ± 18.66	46.53 ± 0.00	<b>47.22 ± 0.00</b>	93.86±0.16	93.40±0.49	<b>94.56 ± 0.71</b>	3
honey-bee-pollen	49.54 ± 1.30	50.00 ± 0.00	<b>56.94 ± 4.53</b>	93.05 ± 0.00	88.89±0.00	<b>93.55 ± 4.53</b>	2
Speed Limit Signs	30.55 ± 2.27	25.00 ± 0.00	<b>31.48 ± 10.23</b>	83.33±0.00	86.11±0.00	<b>90.74 ± 1.31</b>	4
Japanese Characters	0.03±0.00	0.08 ± 0.00	<b>0.50±0.22</b>	53.17 ± 0.15	<b>62.33 ± 0.16</b>	62.16 ± 0.47 0.45	1566

Table 24: Model components and their configuration modes for llma3.2.1B

ID	Name	Type	Params	Mode
0	Model	DiffusionWrapper	102 M	Train
1	Model Ema	LitEma	0	Train
2	First stage Model	VAENoDiscModel	553 M	Eval
3	Cond Stage Model	IdentityCondStage	0	Eval

Table 25: Summary of Experiments for Figures and Tables presented. Min #cls and Max #cls correspond to the minimum and maximum number of classes respectively.

Object	# Datasets	Min #cls	Max #cls	#Params	Trainset Size	Conditioning
Table 1	10	1	5	2565/8005	50k	Dataset
Table 2	5	10	100	128100	20k	Dataset
Table 3	30	19	706	3 M	30	Dataset
Table 4	4	10	10	10853	4	Dataset
Table 5	6	2	3	0.6M	6	Text Description
Table 6	NA	NA	NA	872M	NA	Chunk Indices
Table 7	NA	NA	NA	872M	NA	Chunk Indices
Table 9	2	10	100	0.7M	2	Dataset
Table 11	2	10	100	2048	2	Dataset
Table 15	3	10	1000	1.4M	3	Dataset
Table 16	3	10	100	11M	2	Dataset
Table 16	4	10	10	2.8M	4	Dataset
Table 17	NA	NA	NA	96M	NA	Chunk Indices
Table 18	NA	NA	NA	164M	NA	Chunk Indices
Figure 3	10	2	1566	136468	140	Dataset
Figure 2	2	10	100	0.47M	2	Dataset
Figure 6a	2	10	10	5310	2	Dataset
Figure 7	2	10	10	5310	2	Dataset
Figure 9	5	10	200	2.8M	5	Dataset